Chem Soc Rev

Lanthanide directed synthesis of luminescent self-assembly supramolecular structures and mechanically bonded systems from acyclic coordinating organic ligands

Journal:	*Chemical Society Reviews*
Manuscript ID	CS-TRV-02-2016-000116.R1
Article Type:	Review Article
Date Submitted by the Author:	18-Apr-2016
Complete List of Authors:	Gunnlaugsson, Thorfinnur; Trinity College Dublin, School of Chemistry Barry, Dawn; Trinity College Dublin, Chemistry Caffrey, David; Trinity College Dublin, Chemistry

SCHOLARONE™
Manuscripts

Lanthanide-directed synthesis of luminescent self-assembly supramolecular structures and mechanically bonded systems from acyclic coordinating organic ligands

Dawn Barry,*[a] David F. Caffrey[a] and Thorfinnur Gunnlaugsson*[a]

Received (in XXX, XXX) Xth XXXXXXXXX 20XX, Accepted Xth XXXXXXXXX 20XX
DOI: 10.1039/b000000x

Herein some examples of the use of lanthanide ions (*f*-metal ions) to direct the synthesis of luminescent self-assembly systems (architectures) will be discussed. This area of lanthanide supramolecular chemistry is fast growing, thanks to the unique physical (magnetic and luminescent) and coordination properties of the lanthanides, which are often transferred to the resulting supermolecule. The emphasis herein will be on systems that are luminescent, and hence, generated by using either visibly emitting ions (such as Eu^{III}, Tb^{III} and Sm^{III}) or near infrared emitting ions (like Nd^{III}, Yb^{III} and Er^{III}), formed through the use of templating chemistry, by employing structurally simple ligands, possessing oxygen and nitrogen coordinating moieties. As the lanthanides have high coordination requirements, their use often allows for the formation of coordination compounds and supramolecular systems such as bundles, grids, helicates and interlocked molecules that are not synthetically accessible through the use of other commonly used templating ions such as transition metal ions. Hence, the use of the rare-earth metal ions can lead to the formation of unique and stable species in both solution and in the solid state, as well as functional and responsive structures.

1 Introduction

The objective of this review is to give select examples of the use of the lanthanide ions to direct, or control, the formation of complex supramolecular architectures that have been published over the last decade or so. To date several excellent reviews have been written of the various aspects of the lanthanides,[1-15] these ions which possess rich chemistry that can and has been, in particular, capitalised on in the development of responsive or complex supramolecular structures. The lanthanide ions (Ln^{III}) are a group of elements of the periodic table known as '*rare earth elements*'. They include the 15 elements lanthanum through to lutetium (atomic numbers 57 to 71) and are located between the third row elements barium and hafnium. Contrary to their name, elements such as cerium and lanthanum are found quite abundantly in nature (crustal abundance data: Ce = 66 ppm, La = 35 ppm).[16] Currently the constant requirement to develop new and more efficient magnetic and luminescent materials for application in biomedical analysis, as MRI contrast agents, NMR shift reagents, electroluminescent materials for LEDs, optical fibres for telecommunications and lasers has led to a recent surge of interest in lanthanide ion incorporation in functional supermolecules in order to take advantage of the unique magnetic and photophysical properties these metals have to offer. Several reviews have in the past discussed the photophysical and the coordination properties of the lanthanides, and we direct interested readers to these more extended reviews on these properties.[17,18] Consequently, we will not devote much effort to discuss these herein. Nevertheless, it is necessary to give a brief overview of these to new researchers to the field, interested in discovering and capitalising on these unique properties, as well as some insight into their coordination requirements.

1.1 Some photophysical aspects of the lanthanides

The photophysical properties of the lanthanides are governed by their electronic configurations where a general trend of gradual filling of the 4*f* orbitals is observed. Their electronic configurations are described by $[Xe]4f^n$, where (n = 0-14), as they tend to exist primarily in their trivalent lanthanide state. As electrons successively occupy the valence 4*f* orbitals they do so according to Hund's rule whereby each orbital in the 4*f* sub-shell is singly occupied with one electron before any one orbital is doubly occupied.

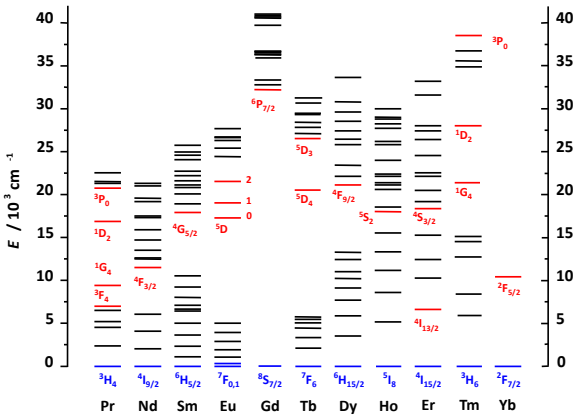

Figure 1. Partial energy diagrams for the lanthanide aquo ions.[19] Reproduced from Ref. 19 with permission from The Royal Society of Chemistry.

Since the 4*f* sub-shell is located in closer proximity to the nuclear core than the outer filled $5s^2\,5p^6$ orbitals poor shielding of

the nuclear charge by the electrons in the 4*f* orbitals leads to a decrease in ionic radii across the series, known as the 'lanthanide contraction', *i.e.* as nuclear charge increases a greater nuclear effect is felt by the $5s^2$ $5p^6$ electrons resulting in a 'contraction' of the ionic radius. This feature gives rise to a similar size and reactivity profile within the lanthanide metal series.[20] As the Ln^{III} 4*f* electrons are located within the filled $5s^2$ and $5p^6$ sub-shells they are 'hidden' from their external environment and so ligand perturbations in the first and second coordination sphere are limited, giving rise to characteristic narrow line-like emission spectra upon Ln^{III} excitation by electromagnetic radiation.[2] Electronic transitions involve a redistribution of electrons within the 4*f* sub-shell, formally Laporte forbidden *f-f* transitions. However, these selection rules may become relaxed by a number of mechanisms such as vibronic coupling (which causes a change in geometry and thus symmetry around the metal ion), *J*-mixing and mixing with opposite parity wave functions such as 5*d* orbitals, and as such weak luminescence results.[17]

The energy gap for Gd^{III} is the largest of all the Ln^{III} with ΔE = 32200 cm^{-1} (for $^6P_{7/2} \rightarrow {}^8S_{7/2}$) corresponding to UV emission, see Figure 1. The most commonly encountered Ln^{III} in luminescent sensor development are Eu^{III} and Tb^{III}, with energy gaps of ΔE = 12300 cm^{-1} (for $^5D_0 \rightarrow {}^7F_6$) and ΔE = 14800 cm^{-1} (for $^5D_4 \rightarrow {}^7F_6$) corresponding to the emission of red and green visible light, respectively. The energy levels of the excited and ground states in Nd^{III} ($^4F_{3/2} \rightarrow {}^4I_J$) and Yb^{III} ($^3F_{5/2} \rightarrow {}^3F_{7/2}$) however are closer together, and so the emission generated is in the near-infrared region of the electromagnetic spectrum.[19]

The Ln^{III} exhibit long luminescence lifetimes, ranging from $10^{-2} \sim 10^{-6}$ s (in the millisecond (ms) range for Eu^{III} and Tb^{III} and the microsecond (μs) range for Sm^{III} and Dy^{III}) compared to those of common organic dyes which are in the nanosecond (ns) range and those of biological media which have excited state lifetimes typically in the sub-microsecond (<μs) range.[2,11,12,21] These two photophysical features offer distinct advantages for responsive probes for cellular imaging and analyte detection in biological media in the development of lanthanide luminescent bioprobes (LLBs) in a technique known as time resolved detection (TRD) or (time-gated detection) where implementation of TRD avoids the detection of short-lived auto-fluorescence from the biological background[22] and light scattering may be avoided, elucidating an intense signal (good signal to noise ratio), as depicted schematically in Figure 2.[5,9] Hence, these are all features highly desirable for the construction of functional supramolecular systems; and often the driving force for the generation of lanthanide based self-assembly structures. However, the drawback is that the formally Laporte forbidden *f-f* transitions accounts for weak absorption extinction coefficients (less than 4 M^{-1} cm^{-1})[7,21,23] and thus low intensity luminescence for such systems.

In order to overcome this obstacle and efficiently populate the lanthanide excited state strongly light absorbing sensitising chromophores are used. These are also known as 'antennae', and may be incorporated into the ligand complexing the lanthanide, or be used as a non-covalently bound coordinating ligand(s). The sensitising antenna(e)'s role is to absorb electromagnetic radiation and transfer this energy to the (triplet) excited state of the lanthanide, generating an excited lanthanide state, where energy is then emitted either as light (luminescence) or undergoes non-radiative deactivation. This indirect excitation of the Ln^{III} excited state allows for the significant photophysical properties of the Ln^{III} to be utilised and probed more efficiently and is known as the 'antenna effect'.[7,19] Energy may be fed onto the Ln^{III} centre by a number of routes, most notably from the triplet excited state of the ligand (T^1) to the Ln^{III} excited state. However, other energy migration pathways have also been encountered such as the direct transfer from the ligand singlet excited state (S^1), intra-ligand charge transfer (ILCT) or ligand-to-metal charge transfer (LMCT) states.[7,19,24] However, these avenues of energy transfer play a less prominent role in the antenna effect, and as such are considered to a much lesser extent.

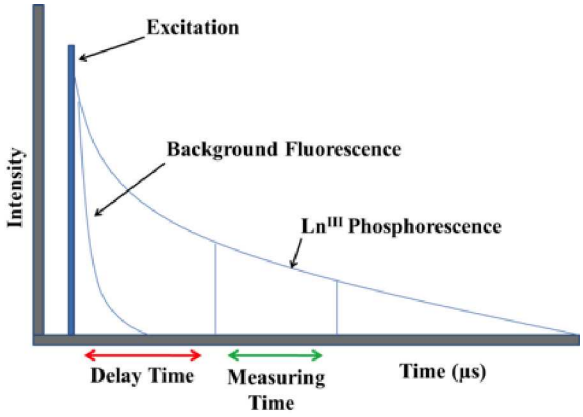

Figure. 2. A time delay between excitation and Ln^{III} phosphorescence detection allows background fluorescence to decay to negligible levels.

Two mechanisms to depict the energy transfer process from the ligand T_1 to the Ln^{III} ion have been commonly accepted and are known as Dexter and Förster mechanisms. The Dexter mechanism involves a double electron exchange whereby, following excitation and subsequent efficient intersystem crossing (ISC), an electron is transferred from the ligand T_1 to the excited state of the Ln^{III}; while simultaneously, an electron is transferred from the highest occupied energy level of the metal ion to the vacant gap created by the initial photo-excitation of the ligand with a distance dependency of e^{-r}. The Förster mechanism, which is more likely for the Ln^{III},[9,19] comprises of energy transfer from the donor to the acceptor *via* dipole-dipole coupling of the dipole moment associated with the de-excitation of the ligand T_1 with the dipole moment associated with the 4*f* orbitals,[8,25] with a distance dependency of r^{-6}, [9,18] (however, it should be noted that higher order terms may also be needed to describe energy transfer between a the ligand T_1 and Ln^{III}). Consequently, for both sensitisation processes, energy transfer is more efficient when the donor antenna group is located in close proximity to the acceptor Ln^{III}. Not only is the efficiency of the sensitisation process dependent on the donor-acceptor distance but it also relies on a number of other factors such as:

1) The energy difference between the antenna S_1 and its T_1 where ΔE = 5000 cm^{-1} is ideal for efficient ISC and thus efficient T_1 population.[17]

2) An optimal energy difference between the antenna T_1 and the Ln^{III} excited state to avoid fluorescence from the antenna (if the energy difference is too high) and non-radiative quenching *via*

back energy transfer (if the energy difference is too low) (for Eu^{III}: 2500 cm^{-1} < ΔE ($^3\pi\pi^*$- $^5D_0$) < 3500 cm^{-1} and for Tb^{III}: 2500 cm^{-1} < ΔE ($^3\pi\pi^*$- $^5D_4$) < 4000 cm^{-1}).[17]

3) Minimisation of deactivation by non-radiative processes such as vibrational collisions with local solvent molecules, known as quenching.[25,26] Although it must also be taken into consideration that the presence of some close diffusing vibrational oscillators are essential to sensitising emission, since they can act to allow phonon assistance (low phonon systems with no suitable vibrational manifold (such as polyoxometallates) don't generally exhibit effective sensitised emission behaviour).

The dependence of Ln^{III} luminescence on the above parameters means that careful ligand design for appropriate Ln^{III} complexation and sensitisation must be taken into account to achieve full exposure of the photophysical properties of the Ln^{III} in the formation of novel applicable lanthanide luminescent systems.

1.2 The coordination chemistry of the lanthanides

Ionisation energy data reveal that the lanthanides exist primarily in their +3 oxidation state with high charge density causing them to act as hard Lewis acids. They tend to possess variable and large coordination numbers (from between 9 and 12) forming labile ionic complexes with donor ligands which are hard Lewis bases.[16] The development of systems incorporating the Ln^{III} therefore entail the design of ligands containing functional groups such as amides, carboxylates and nitrogen based heterocycles that facilitate their high coordination requirements.[16,21] Moreover, it is essential that ligand-Ln^{III} bond formation results in both kinetically and thermodynamically stable complex formation to ensure that the Ln^{III} remains tightly bound. Unfavourable enthalpic processes such as ligand dehydration in solution are generally not counteracted by favourable ligand-Ln^{III} bond formation and it is thus understood that the assembly process and subsequent bond formation is entropically driven.[4,19] Polydentate acyclic chelating ligands such as podands offer enhanced stability over monodentate ligands due to the 'chelate effect' (*i.e.* reduced entropy of disorder loss and ring formation upon complexation). In such instances a number of flexible functionalised pendant arms containing appropriately located coordinating groups (usually bidentate/tridentate) are generally grafted onto such structures in a pre-organised manner for Ln^{III} encapsulation.[19,27-29,] However, this strategy lacks the pre-disposition macrocyclic ligands have to offer as complexation requires a large conformational entropic factor in comparison. Polydentate macrocyclic ligands containing a pre-organised cavity, such as cyclen[30-32] and calixarenes,[33] further reduce the entropic cost compared to their acyclic counterparts by maintaining a pre-determined cavity size and optimised coordinating sites for Ln^{III} selectivity. This is known as the 'macrocyclic effect', a specific case of the 'chelate effect'. Furthermore, pendent arms are often attached to the cavity encouraging further pre-organisation, as the arms are available to assemble and ensure coordinative saturation and Ln^{III} stability. Another strategy implemented to develop more sophisticated complex supramolecular systems is that of self-assembly. Self-assembly comprises of the fine tuning of ligand design such that complimentary weak non-covalent interactions drive the manifestation of hierarchal molecular edifices.[34] By pre-organising ligands in a specific manner one can take advantage of the intermolecular forces between functional groups on adjacent ligands and control the assembly of these coordinating building blocks around one or several ions. This self-assembly process has led to the generation of elegant systems such as catenanes, rotaxanes,[35-40] metal-directed molecular cages and boxes.[41] Whilst much emphasis has been placed on the development of transition metal based supramolecular systems[37,42-46] Ln^{III}-directed self-assembly formation has only recently experienced considerable attention, offering a route towards large molecular fabrications such as bundles, helicates or hierarchical systems such as clusters or metal organic frameworks (MOFs).[47-55] Since the Ln^{III} possess larger coordination numbers than the transition metal ions, ligand binding sites and metal coordination geometries play an even more important role in determining and controlling the overall structure of the resulting system.

The purpose of this review is to compliment previous review articles on this topic by highlighting new advances made to the area. The first section discusses new developments made to monometallic *f*-block self-assembly superstructures formed from acyclic ligands while the following section details advances made to multimetallic self-assemblies such as clusters, grids, helicates and MOFs. Only a few examples of interlocked structures driven by Ln^{III} coordination exist, which is discussed in the final section.

2 Monometallic self-assembly structures from acyclic ligands

2.1 Dipicolinic acid and benzimidazole-pyridine ligands

Jean-Claude Bünzli, one of the foremost leaders in supramolecular Ln^{III} chemistry, has dedicated tremendous research efforts to the design and synthesis of metal-directed Ln^{III} self-assemblies, accomplished typically by derivation of the dipicolinic acid (dpa) ligand core **1**. The extensive employment of the H_2dpa backbone as a Ln^{III} chelating unit originates from its ability to form nine-coordinate 1:3 (Ln:dpa) tris(dipicolinate) complexes bearing high stability constants.[56] The crystal structures of many such complexes have been reported[57,58] while the capacity of H_2dpa, **1**, to deliver sufficient photophysical properties for efficient lanthanide luminescent sensitisation encourages its continued study and derivatisation for further application. Relatively large luminescent quantum yields are exhibited by, in particular, Eu^{III} and Tb^{III} tris(dipicolinates) where $Cs_3[Eu(dpa)_3]$ and $Cs_3[Tb(dpa)_3]$ for example display quantum yields of 24% ± 2.5% and 22% ± 2.5%, respectively, in TRIS-HCl buffered solution (0.1 M).

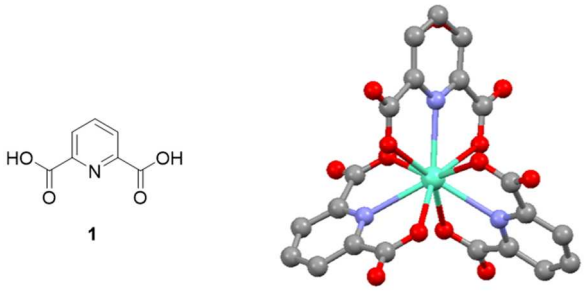

Figure 3. 2,6-pyridinedicarboxylic acid (H_2dpa) **1** and X-ray crystal structure of $Cs_3[Eu(\mathbf{1})_3]$ reproduced from ref 57. Hydrogen atoms have been omitted for clarity.

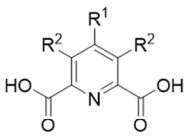

2: R^1 = OH, R^2 = H
3: R^1 = Cl, R^2 = H
4: R^1 = OH, R^2 = Br

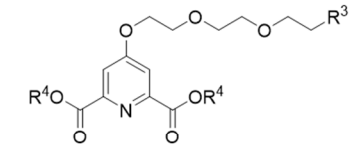

5: R^3 = OMe, R^4 = H
6: R^3 = OH, R^4 = Na
7: R^3 = NH_2, R^4 = H
8: R^3 = Phta, R^4 = Na

Phta:

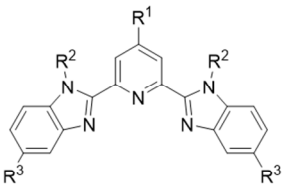

9: R^1 = H, R^2 = CH_3, R^3 = H
10: R^1 = H, R^2 = C_2H_5, R^3 = H 10
11: R^1 = H, R^2 = C_8H_{17}, R^3 = H
12: R^1 = H, R^2 = $(CH_3O)_2C_6H_3$, R^3 = H
13: R^1 = C_6H_5, R^2 = $(CH_3O)_2C_6H_3$, R^3 = H

The intense luminescence observed is a result of sensitisation occurring through the dpa^{2-} triplet excited state with an efficiency of 85% for the tris complex in the solid state and 61% in solution and as such these systems have been proposed by Chauvin *et al.* for implementation as secondary standards for quantum yield determination.[59]

George *et al*. reported the synthesis of H_2dpa (**1**) analogues **2** - **4** where the 4 and 3, 5 positions of the pyridine ring were derivatised with hydroxy, chloro and bromo substituents.[60] A photophysical study was carried out to investigate the effect these simple modifications have on the sensitisation and emission properties of the Eu(**L**)$_3$ (where **L** = **1** - **3**) and Eu(**4**) complexes. Findings were compared to results previously reported for analogous Tb^{III} systems and following substitution of the four position in the order Cl > H > OH it was found that the ability to sensitise Eu^{III} emission was increased, in contrast to OH > H > Cl for Tb^{III}.[61] In the case of **4**, the dibromo-4-hydroxy derivative, no sensitisation was observed and so results were inconclusive due to incomplete saturation of the Eu^{III} coordination sphere as a Eu:**L** ratio of 1:1 was found. Long luminescence lifetimes were also determined for Eu(**L**)$_3$ (where **L** = **1** - **3**) ranging from 1.16 to 2.9 ms (in CH_3OH and H_2O) - an attractive feature for the development of luminescent biological probes.

Chauvin *et al.* synthesised four novel derivatives of H_2dpa where the 4-*para* position of the pyridine unit was functionalised with a polyethylene chain, each chain differing by the terminal group, to react with Eu^{III} and Tb^{III} forming tris chelate complexes.[62] Not only did these ligands form thermodynamically stable 1:3 monometallic complexes at physiological pH ($\log\beta_{13} \approx$ 19 – 20 (Eu(**L**)$_3$); **L** = **5** - **8**) but also, depending on the terminal substituent of the pendant arm, the photophysical properties were tuned. Substitution at the 4-*para* position always displayed a detrimental effect on Tb^{III} sensitisation where luminescence quantum yields (in H_2O) did not exceed 18%, compared to that of 22% for $[Tb(\mathbf{1})_3]^{3-}$. Nevertheless, sensitising efficiencies of 70% gave rise to quantum yields of up to 29% (for **L** = **7**) for the Eu^{III} tris complexes, 5% larger than that observed for $[Eu(\mathbf{1})_3]$.

The bis(benzimidazole)pyridine tridentate ligand has been intensively investigated and implemented for the formation of both mononuclear and multinuclear Ln^{III}-directed self-assembled systems, by both Bünzli, Piguet and co-workers, in which a large library of precursors have been synthesized and studied (five examples of which are shown **9** – **13**), bearing substituents of varying steric and electronic character appended to different positions of both the pyridine and benzimidazole subunits.[63-68] The effect the incorporation of such substituents has on the photophysical characteristics and overall size and shape of the final mononuclear system was evaluated. Ligands **9** – **11** were reacted with lanthanide nitrates to give neutral 1:1 nitrato luminescent

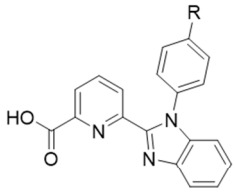

14: R = H
15: R = Br
16: R = ^{t}Bu
17: R = OC_8H_{17}

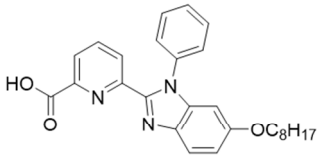

18

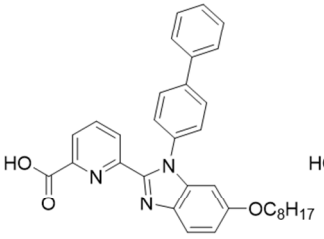

19

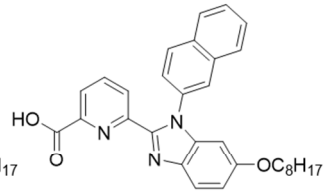

20

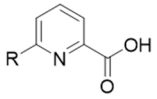

21: R = $PO(OEt)_2$
22: R = PO(OEt)OH
23: R = $PO(OH)_2$

complexes $[Ln(NO_3)_3(\mathbf{L})(solv)]$ (**L** = **9** – **11**, & **13**) while simply choosing non-competitive lanthanide perchlorate salts instead yielded tris $[Ln(\mathbf{L})_3]^{3+}$ (**L** = **9** – **12**) complexes with a coordination geometry close to the ideal tricapped trigonal prism. It has been established, from these in depth studies, that substitution at the R^3 position of the ring dictates the electronic and photophysical properties of the final complex system while

substitutions at R^1 and R^2 influences its overall structure and stability as steric bulk at these positions affects the co-planarity of the aromatic rings in the final complexes, severely limiting their stabilities in solution. [63-68]

In addition to the bis(benzimidazole)pyridine ligands, mono derivatised benzothiazole-, benzoxazole- and benzimidazole-substituted pyridine-2-carboxylic acids have also been shown to be capable of providing a nine-coordinate environment for the Ln^{III}.[69-72]

The assembly of benzimidazole pyridine-2-carboxylic acid ligands (**14** – **20**) with Eu^{III} where again shown to give discrete mononuclear complexes of 1:3 stoichiometry. X-ray crystallographic studies showed the structures of these Eu^{III} complexes to be acutely similar to those of *N*-alkyl analogues published previously, despite the increased steric bulk.[71] The global objective of this work, however, was to ascertain the influence of ligand structure on the luminescence quantum yield. *Para*-substitution of the *N*-phenyl ring in **14** – **17** was proven to have no effect on quantum yield, even though perturbation of the ligand triplet states had occurred. In contrast, a marked reduction in quantum yield was observed upon grafting an octyl chain at the C-6 atom of the benzimidazole antenna (**18** – **20**), suggesting future modification would be best situated at the *N*-alkyl group considering the negligible effect on the Eu^{III} luminescence.

6-Phosphoryl picolinic acid derivatives (**21** - **23**), in which one of the carboxylate side groups of **1** has been replaced by a phosphoryl-based functional group, have quite recently been published with compounds **21** and **22** shown to form water soluble 1:3 Eu:**L** and Tb:**L** complexes. Complexes of **23**, however, precipitate in the presence of Ln^{III}.[73] Stability constants greater than those observed for the parent H_2dpa compound were determined where $\log\beta_{13}$ = 23.8 and 24.3 for $Eu(\mathbf{21})_3$ and $[Eu(\mathbf{22})_3]^{3-}$ were calculated, respectively, in comparison to $\log\beta_{13}$ = 22.4 for $[Eu(\mathbf{1})_3]^{3-}$. The emission spectra of $Eu(\mathbf{21})_3$ and $[Eu(\mathbf{22})_3]^{3-}$ were also measured as a function of pH (in a 0.1 M KCl solution) displaying the highest luminescence at pH 4.8 for $Eu(\mathbf{21})_3$ whereas $[Eu(\mathbf{22})_3]^{3-}$ was more luminescent at pH 9.0. Obtaining maximum emission at these pH extremities is uncommon yet quite interesting for self-assembled systems of this nature. [73]

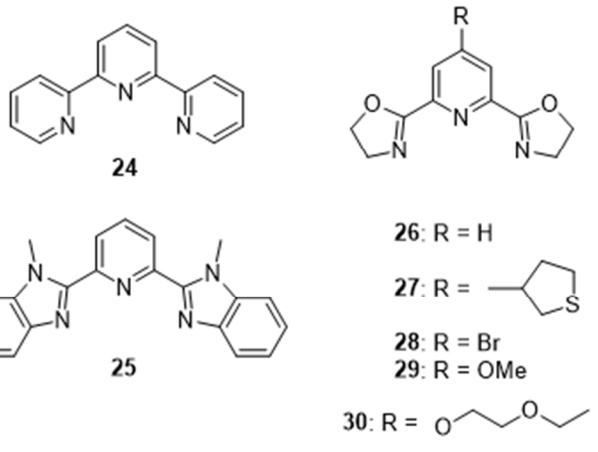

Piguet and co-workers have long been concerned with probing the thermodynamic and steric parameters that dictate the final structure and corresponding stability of metal-driven self-assemblies. In 2009, studies were extended to the investigation of tridentate terpyridine (**24**) and 2,6-bis(1-methylbenzimidazol-2-yl)pyridine (**25**) chelating ligands, whose formation of triple-helical bundles was, by way of repulsive interligand interactions that serve to destabilize the complex, deemed to be anti-cooperative both in solution and in the solid state.[63] Their findings have brought them to conclude that complexation of **24** and **25**, each adapted for producing planar 1:1 and helical 1:2 and 1:3 (Ln:**L**) stoichiometric complexes with Ln^{III} ions, was especially sensitive to solvation effects and the nature of the counter-anion. Moreover, the larger coordination cavity offered by **25** compared to **24** generated 1:3 species of improved stability and kinetic inertness.

2.2 Pybox and other pyridine-based ligands

Pyridine-bis(oxazoline) ligands, also known as Pybox (**26**), are another class of simple precursors which have shown promise as competent chromophores for Ln^{III} sensitisation. The thiopene-derivatised-Pybox, **27**, was the first published Pybox Ln^{III} sensitizer forming 1:1, 1:2 and the 1:3 (Ln:**L**) species in CH_3CN solution.[74] Substantial quantum yields (in CH_3CN) of 76% and 59% for $Eu(\mathbf{27})_3$ and $Tb(\mathbf{27})_3$ and a 1:2 crystal structure of the $Eu(\mathbf{27})_2$ species were obtained. This further fuelled the progressive study and modification of the Pybox framework eventually leading to the evolution of compounds **28** and **29**. An electron donating methoxy and an electron withdrawing bromo moiety were attached to the 4-*para* pyridyl position of Pybox for comparison with the parent Pybox ligand **26** as well as the previously developed **27**. A number of crystals suitable for X-ray diffraction were grown and in most cases displayed the anticipated 1:3 stoichiometries for these examples. Solution studies in CH_3CN also evidenced the existence of the 1:1, 1:2 and the 1:3 (Ln:**L**) species, while appreciable quantum yield values were obtained for these in CH_3CN (for $Eu(\mathbf{28})_3$ = 36%, $Tb(\mathbf{28})_3$ = 23%, $Eu(\mathbf{29})_3$ = 24% and $Tb(\mathbf{29})_3$ = 21%).[75] Furthermore, subsequent tailoring of the Pybox structure, by attachment of an ethylene glycolethyl ether to the 4-*para* position afforded **30** and successfully demonstrated the ability of these Pybox ligands to sensitise the Ln^{III} in a fully aqueous environment.

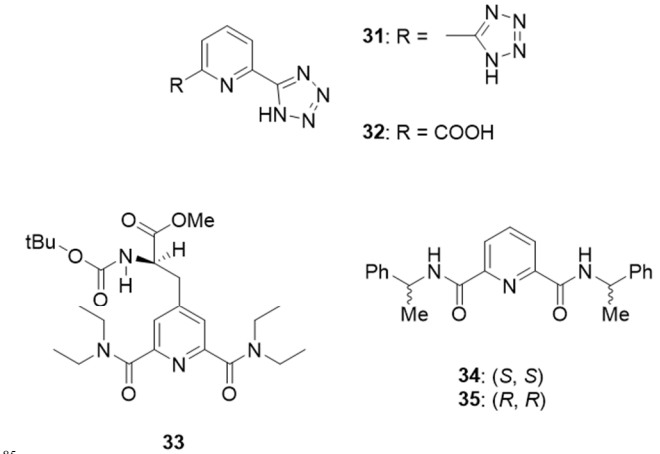

Other *N*-donor chelating units, which have been employed for Ln^{III}-coordination include 2,2'-bipyridine,[76-78] 2,6-bis(1,2,3-triazol-4-yl)pyridine (btp),[79-83] 2,6-di(pyrazolyl)pyridines (bpp),[84,85] 2,2';6',2''-terpyridine (terpy),[86-89] and quite recently tetrazole ligands, two examples of which, published by Mazzanti *et al.*, are discussed below.[90-92]

Both tridentate chelating building blocks **31** and **32** were shown to form helical tris-chelate Ln^{III} complexes, as evidenced by structural analysis and ^{1}H NMR analysis. It was also found that by changing the counterion for these assemblies the solubility of both complexes could be tuned. Of these, the bis-tetrazolate-pyridine ligand **31** offered the most promising photophysical properties as it was not only capable of sensitizing both visible and near-IR emitting Ln^{III} but the absorption window of the corresponding complexes were also significantly extended towards the visible region (up to 330 nm), relative to the parent H_2dpa system itself.[91].

Derivatization of the 4-*para* position of **31** with a triazole unit has led to a more optimized energy transfer pathway, yielding 1:3 (Ln:**L**) complexes with very high luminescent quantum yields (up to 70% for Eu and 98% for Tb in the solid state).[93] A more recent publication by the same group details a series of related tetrazolate scaffolds functionalised at the 4-*para* position of the pyridine ring and the effect these substituents have on the photophysical properties of the ligands and its corresponding 1:3 (Ln:**L**) complexes (Ln = Eu^{III}, Gd^{III} and Tb^{III}) [94]

2.3 Chiral amido-pyridine ligands

Crucial to modern drug discovery is the recognition of chiral molecules, the determination of the absolute configuration of an unknown chiral compound.[95] Since the observation of the Pfeiffer effect - the induction of optical activity in a solution of a labile racemic mixture by the addition of a secondary chiral substance,[96] a growing interest in the development of chiral luminescent probes has occurred and led to the generation of monometallic Ln^{III}-directed self-assemblies of **33**, **34** and **35**.[97-99]

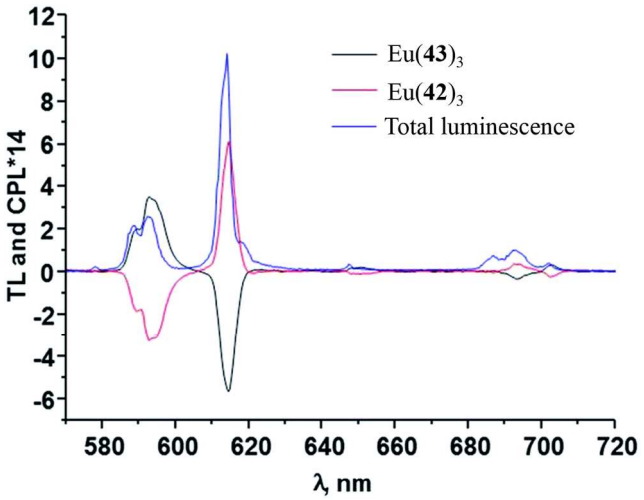

Figure 4. The CPL spectra for Eu**42**$_3$ and Eu.**43**$_3$ in CH_3OH; the total luminescence is also shown. Reproduced from ref. 102 with permission from The Royal Society of Chemistry.

In luminescent Ln^{III} complexes ligand field structure is sensitively reflected in the sign and magnitude of Circularly Polarized Luminescence (CPL) and therefore CPL active Ln^{III} complexes have potential use in chiral sensing and imaging applications.[100] The advantage of using luminescent Ln^{III} complexes as chiroptical probes is that large luminescent dissymmetry values (g_{lum}) as high as 0.5 may be observed for selected Ln^{III} transitions compared to other chiral organic molecules for which the extent of circular polarization is less than 1 x 10^{-2}.[100,101] See Figure 4 for CPL spectra of complexes Eu(**42**)$_3$ and Eu(**43**)$_3$ (discussed below), which correspond to g_{lum} values of -0.15 and 0.16 for the $^5D_0 \rightarrow {}^7F_1$ transition of Eu(**42**)$_3$ and Eu(**43**)$_3$, respectively.[102]

Preliminary studies in this discipline have elucidated that **33**, a tridentate ligand bearing a bulky chiral group in the 4-*para* position of the pyridine ring, forms thermodynamically stable $[Ln(\mathbf{33}_3]^{3+}$ (Ln = La^{III}, Eu^{III}, Lu^{III}) complexes in CH_3CN with $\log_\beta$ values in the range 19-20. However, only a very small excess of one diastereoisomer was induced in solution, reflected by weak CPL signals for $[Eu(\mathbf{33})_3]^{3+}$ and $[Tb(\mathbf{33})_3]^{3+}$ (calculated luminescence dissymmetry factor for $[Tb(\mathbf{33})_3]^{3+}$ $^5D_4 \rightarrow {}^7F_5$ transition g_{lum} = 0.02).[98,99] This result encourages the introduction of more influential functional groups capable of inducing pronounced diastereoisomerism in such structures.

Enantiomers **34** and **35** were shown to form stable 1:3 $[Eu(\mathbf{L})_3]^{3+}$ (**L** = **34**, **35**) optical isomers *in situ* possessing constant CPL activity over a long period of time in CH_3CN (calculated luminescence dissymmetry factor for $[Eu(\mathbf{34})_3]^{3+}$ $^5D_0 \rightarrow {}^7F_1$ transition g_{lum} = 0.19).[97,99] Due to the long shelf life exhibited by these chiral emitting species they have been proposed as reliable CPL calibration standards. Further study on these systems have revealed the formation of stable tris complexes in CH_3CN (logβ in the range 23.8) while X-ray crystal structures of $[Ln(\mathbf{L})_3]^{3+}$ (**L** = **34**, **35**; (Ln = Eu^{III}, Gd^{III}, Tb^{III} and Yb^{III}) are isostructural for the Ln^{III} series studied in the solid state. Most importantly, this study illustrates that the chiral nature of the ligand may induce Δ or Λ stereochemistry in the final complex product. Attentive ligand design may therefore be exploited to build upon these chiral Ln^{III} complex bioprobe foundations.

Chiral self-assembled monometallic 1:3 (Ln:**L**) bundle systems, known as the 'Trinity Sliotar', have received considerable attention within our laboratory. In the original Trinity Sliotar system three pyridyldiamide tridentate chelating ligands (**36** or **37**) are organised around a Ln^{III} (Ln^{III} = Nd^{III}, Sm^{III}, Eu^{III}, Tb^{III}, and Yb^{III}) centre in a tightly packed helical manner,[52] with each ligand bearing two chiral naphthalene antenna. The 1:3 (Ln:**L**) complexes were found to be highly symmetrical, with the ligand chirality transferred to the complex upon self-assembly, as evidenced by CD, CPL and X-ray crystallography, to give either Δ or Λ stereoisomers. Solid state X-ray crystallography confirmed the appreciable stability of these bundles, as face-to-face π-π stacking interactions existed between the pyridine unit of one ligand and one naphthalene unit from each of the other ligands upon complexation. Both excited state lifetime measurements and X-ray crystallography confirmed that the Ln^{III} sits in a fully saturated coordinative environment, see Figure 5(A).[52,103]

Although factors such as thermodynamic stability, kinetic inertness, sizable luminescence quantum yields and long excited state lifetimes – prime specifications for the construction of Ln^{III} containing luminescent devices – were appreciable for complexes of **36** and **37** it was crucial to fully elucidate the extent to which these systems could be modified and how minor changes to the original structure might influence these parameters. Consequently, the symmetrical 2-naphthalene isomers **38** and **39**, and the asymmetrical pyridyl ligands **40 - 43 -** (discussed below) were synthesised by our research group in order to probe such queries.

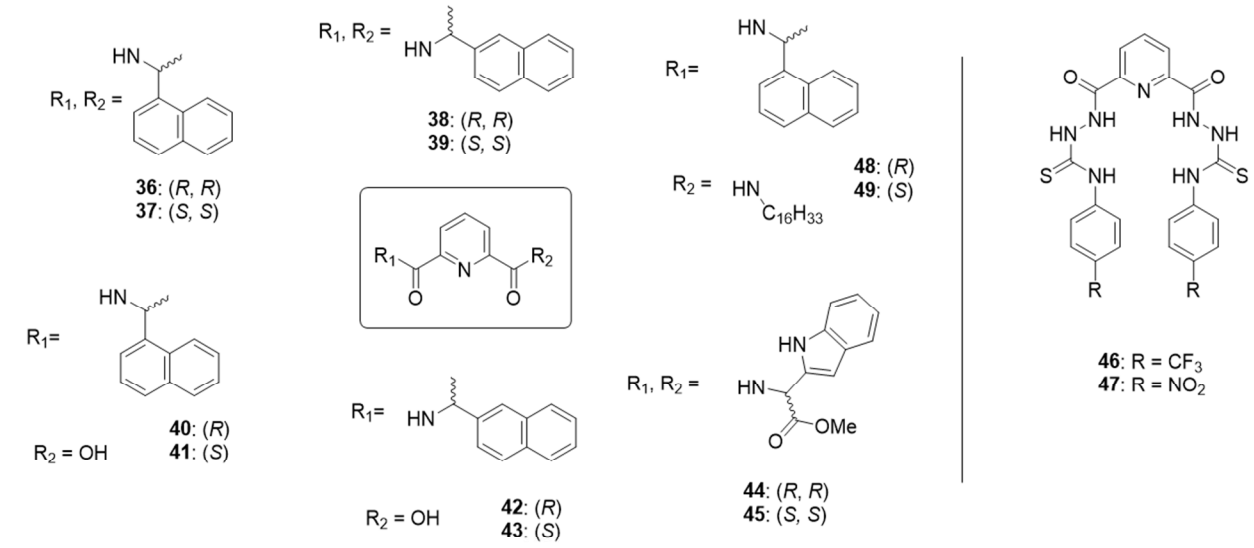

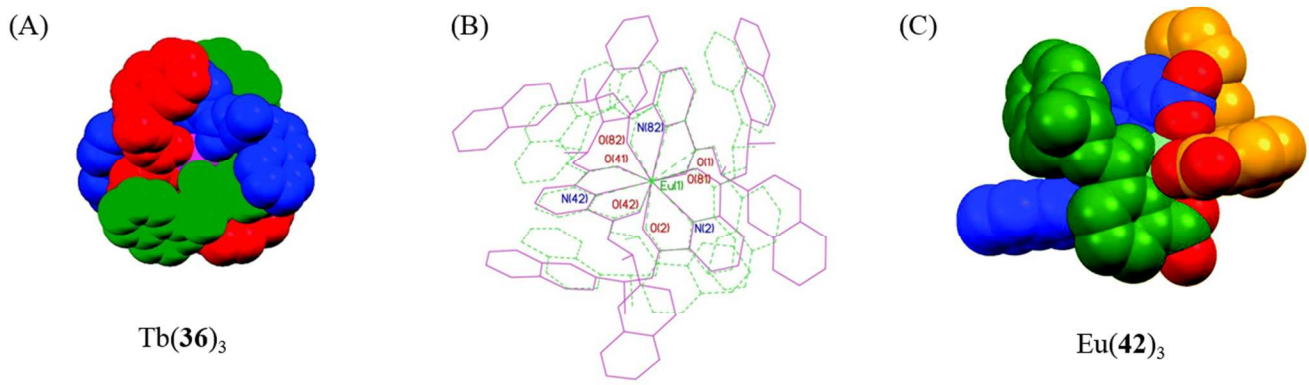

Figure 5. Compound structures **36** – **47** and (A) the X-ray crystal structure of the Tb(**36**)$_3$ sliotar as viewed down the crystallographic *c*-axis (reprinted with permission from Ref. 52. Copyright (2007) American Chemical Society). (B) Overlay figure of Eu(**38**)$_3$ (solid lines) with Eu(**36**)$_3$ complex (dashed lines). (Reproduced from ref. 103 with permission from John Wiley & Sons). (C) Space filling representation of Eu(**42**)$_3$ complex (reproduced from Ref. 102 with permission from The Royal Society of Chemistry) showing the position of carboxyl oxygen atoms (in red) relative to the naphthyl antennae. H-atoms, solvent molecules, and counter anions omitted for clarity.

Synthesis and spectroscopic studies were conducted on ligands **38** and **39** with Eu^{III} only and compared to previously documented results for **36** and **37**.[103] X-ray crystal structures of the enantiomeric pair Eu(**L**)$_3$(ClO_4)$_3$ (**L** = **38**, **39**) were grown and shown to be isostructural to one another, similarly to the enantiomeric triflate complex pair of **36** and **37**. In contrast, π-π stacking, which is responsible for the tightly packed nature of the Eu(**L**)$_3$(CF_3SO_3)$_3$ (**L** = **36**, **37**) complexes, was not observed for Eu(**L**)$_3$(ClO_4)$_3$ (**L** = **38**, **39**) giving rise to a more flattened and open structure, see Figure 5(B). This subtle change to the original framework not only plays a role in dictating the structure of the solid state but self-assembly stability and complex photophysical features were also affected. Thermodynamic stability constants obtained from spectroscopic investigations of the 1:3 Eu:**L** (**L** = **38**, **39**) self-assembly species were comparable to those obtained for **36** and **37** in CH_3CN ($\log\beta_{13} \approx 20$) however in protic CH_3OH solution a decrease in stability was evident from the reduction in $\log\beta_{13}$ values from $\log\beta_{13} \approx 19$ for Eu(**L**)$_3$ (**L** = **36**, **37**) to $\log\beta_{13} \approx 17$ for Eu(**L**)$_3$ (**L** = **38**, **39**). The higher binding constants obtained for the Eu^{III} tris complexes with **36** and **37** were attributed to the presence of stabilising π-π stacking interactions in the 1-naphthyl derivatives. It has to be stated that the solvation effects can also play an important role in the desolvation of ligands which can

also affect the binding model. Luminescence quantum yields were measured and antenna-to-ion energy transfer (η_{sens}) values calculated with Φ_{tot} found to be four times higher for Eu(**L**)$_3$ (**L** = 3**6**, **37**) than for Eu(**L**)$_3$ (**L** = **38**, **39**) in both solvents. These values confirm that the efficiency of sensitisation is in fact five times less for Eu(**L**)$_3$ (**L** = **38**, **39**).

Carrying only a single naphthalene chromophore, the optically active ligand pair **40** and **41** were developed as asymmetrical analogues of **36** and **37**.[104] Utilizing photophysical analysis, **40** (*S*) and **41** (*S*) were shown to form 1:3 (Ln:**L**) complexes with Eu^{III} in CH_3CN with high stability constants ($\log_\beta$ = 19.7 and 19.8 for Eu.**40**$_3$ and **41**$_3$, respectively) and as single chiral geometrical isomers in solution. Upon the addition of 0.33 equivalents of Eu^{III} luminescence intensity maxima was observed for both ligands, evidencing the favoured formation of Eu.**L**$_3$ (**L** = **40** and **41**) in solution. Molecular modelling calculations (MM2) were also implemented with results from these calculations indicating that all three naphthalene antennae were residing on the same side of the 1:3 structure, directed towards the inside of a "half-helicate", with the methyl groups outside the coordination sphere of the Ln^{III} ion.

The 2-naphthyl enantiomeric pair **42** and **43**, isomers of **40** and **41**, have also been employed for the Ln-directed synthesis of chiral luminescent half-helicate structures.[102] The successive formation of the Eu.**L**$_1$, Eu.**L**$_2$ and the Eu.**L**$_3$ (**L** = **42** and **43**) species was observed in CH_3CN upon the addition of $Eu(CF_3SO_3)_3$ with binding constants found to be lower ($\log_{\beta 13}$ = 16.5 and 17.3 for Eu.**42**$_3$ and Eu.**43**$_3$, respectively) than those calculated for the analogous 'Trinity Sliotar' and other similar systems.[52,103,104] Confirming the MM2 calculations for **40** and **41** above, a crystal structure of Eu.**42**$_3$ was grown and analysed by X-ray crystallography, showing the ligands arranged around the Eu^{III} centre with the three naphthyl antennae located on the same side, see Figure 5(C). Most notable from this study was the application of chiroptical spectroscopy in quantifying the binding events of the self-assembly process. Non-linear regression analysis of the circular dichroism (CD) titration data elucidated binding constants which compared comfortably with those obtained from traditional spectroscopic methods and gave unique insight into the self-assembly formation in solution.

The effect replacing the naphthalene functionality with the biologically relevant tryptophan group has on the self-assembly process has also been investigated for these chelating tridentate ligands. Mass spectrometry and fitting of spectroscopic data, obtained following the addition of either $Eu(CF_3SO_3)_3$ or $Tb(CF_3SO_3)_3$ to **44** or **45** in CH_3CN, suggested the formation of only the 1:1 and the 1:2 (Ln:**L**) species in solution but not the predicted 1:3 species. It was concluded from this study that the absence of the 1:3 species may either be due to steric hindrance or participation of two additional donor atoms from the amino ester functionality fully occupying the coordination sphere of the Ln^{III}. In this instance, the structural integrity of the bundle analogue has been shown to impede the stoichiometry of the system as neither Tb^{III} nor Eu^{III} directed the formation of the expected 1:3 nine-coordinate complex in solution.

2.4 Applications of monometallic self-assemblies

Evidently a great deal of knowledge has been gained for these particular coordinating ligands where a library of derivatives have been synthesized and spectroscopically evaluated in order to gain insight into their behaviour as potential Ln^{III} sensitizers for luminescent self-assemblies. However, in addition to designing novel Ln^{III} sensitizers for *f*-block directed assembly, the creation of functional molecular structures is highly attractive for the construction of new materials and technologies. As a result of structural and functional integration of supramolecular (chemical) entities, exciting new developments have emerged in applications as far afield as molecular machinery to biological cell imaging agents and analytical optical sensing. For example, by attaching a dibenzo[24]crown-8 functionality to the 4-pyridyl position of the dpa core Liu and co-workers have developed a 1:3 (Tb:**L**) luminescent lanthanide pseudorotaxane, which, through the threading and de-threading of a benzyl(ferrocenylmethyl)ammonium moiety, acts as a reversible optical switch.[105]

By combining the diamido pyridyl tridentate O^N^O (NO_2) Ln^{III} binding unit with the amidothiourea moiety, a proven colorimetric sensor of anions in aqueous media, it was envisaged that such a design would enable the luminescent properties of 1:3 (Ln:**L**) mononuclear Ln^{III}-directed self-assemblies to be exploited for optical sensing purposes, instilling an applicable function in systems of this type.[106] With this in mind the symmetric pyridyl bis-amidothiourea based ligands **46** and **47** were synthesized and, following formation of the 1:3 (Tb.**L**$_3$, **L** = **46** and **47**) species *in situ*, modulation of the Tb^{III}-centred emission was observed upon recognition of the anions acetate and phosphate in DMSO-H_2O (4:1) solutions. Much emphasis is being placed on tailoring efficient Ln^{III} sensitizing ligands for use as solution-based analytical tools, however, a surge of interest in the fabrication and generation of solid state Ln^{III} luminescent assemblies exists.

Currently, from a materials aspect, we are focusing on the use of the Langmuir and Langmuir-Blodgett (LB) technique and generation of soft materials. The LB technique allows for the translation from solution to the solid state with the additional benefit of offering control, at the molecular level, over organization into thin monomolecular films. Deposition of Ln^{III} systems of this nature onto solid supports in this manner is opening up new prospects for optical sensing applications.

A hydrophobic alkyl hydrocarbon chain was grafted onto the 6 pyridyl position of the enantiomeric pair **40** and **41**, affording **48** and **49**, in order to induce sufficient amphiphilicity for monolayer formation at an air-water interface and subsequent immobilization onto a quartz substrate for the generation of solid state emissive materials. Following spectroscopic investigations of the self-assembly process of **48** and **49** with Ln^{III} metal ions in CH_3CN (where Ln^{III} = Eu^{III} and Nd^{III}) the 1:3 Ln.**L**$_3$ complexes were synthesized and each assembled into monomolecular thin films at the air-water interface.[107,108] Subsequent immobilization onto a quartz slide generated luminescent thin films; and in the case of Eu.**48**$_3$ and Eu.**49**$_3$, exhibition of CPL activity - representing the first examples of Ln^{III} CPL emitting amphiphilic self-assemblies. This work is an ongoing area of research we are continuously investigating with studies incorporating other Ln^{III} being carried out with adjustments to the current amphiphilic ligands **48** and **49** currently underway. In addition to the LB technique, a substantial effort to strategically incorporate Ln

luminescent systems into solid supports, such as gold nanoparticles and gels, [109-115] is being carried out.

Mimicking biological systems, such as the healing of broken bones or injury to blood vessels, self-healing materials are of great interest as they can self-repair damage and regenerate function, extending the life-span of the material. Luminescent self-assembled supramolecular metallogels, based on **50**, were generated and shown to display this self-healing feature, see Figure 6. Employing the NO_2 pyridyl diamide tridentate binding moiety as before it was expected that the 1:1 1:2 and 1:3 (Ln:**L**) metal-directed species would assemble in solution, as had been observed previously for analogous systems. Spectroscopic studies conducted in CH_3CN, using $Ln(CF_3SO_3)_3$ (Ln = Eu^{III} and Tb^{III}), did indeed reveal the expected stoichiometric species with binding constant values of $\log_{\beta 1:1} = 6.7$, $\log_{\beta 1:2} = 14.2$ and $\log_{\beta 1:3} = 21.0$

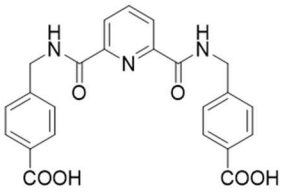

50

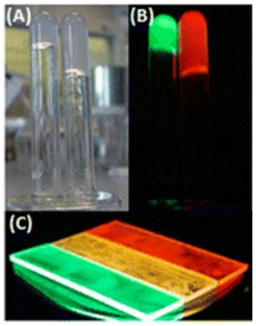

Figure 6. Compound **50** and corresponding Eu^{III} and Tb^{III} gels (A) in day light and (B) their luminescence under UV light. (C) Luminescence of Eu^{III}, Tb^{III}, and Eu^{III}/Tb^{III} gels on quartz plates (reprinted with permission from Ref. 116. Copyright (2015) American Chemical Society).

determined for the Eu^{III} species while $\log_{\beta 1:1} = 6.9$, $\log_{\beta 1:2} = 13.$ and $\log_{\beta 1:3} = 18.7$ were calculated for the Tb^{III} species.[116]

However, following titrations carried out in CH_3OH, photophysical changes were satisfyingly fitted to 1:1, 1:2, 2:2 and 3:2 (Ln:**L**) stoichiometries, with no reliable fit obtainable for the 1:3 assembly (binding constant values of $\log_{\beta 1:2} = 12.2$, $\log_{\beta 2:2} = 18.9$ and $\log_{\beta 3:2} = 25.2$ for the Eu^{III} species and $\log_{\beta 1:2} = 12.4$, $\log_{\beta 2:2} = 19.7$, $\log_{\beta 3:2} = 24.0$ for the Tb^{III} system were calculated). Moreover, NMR studies further indicated an initial assembly of the 1:3 (Ln:**L**) stoichiometric species, followed by the formation of a higher-order polymer as additional metal ions were added and cross-linked through the carboxylic acid connections. Following these solution based results, supramolecular gels were prepared by firstly reacting ~ 10mM of **50** with $Ln(CF_3SO_3)_3$ (Ln = Eu^{III} or Tb^{III}) in a 1:3 (Ln:**L**) stoichiometric ratio under microwave irradiation at 75 ^oC for 20 mins. It was found that the addition of 0.5 equiv. of $Ln(CH_3COO)_3$ (Ln = Eu^{III} or Tb^{III}) to this solution gave rise to a stable robust gel after centrifugation or by leaving to stand at room temperature overnight. These gels were found to be highly luminescent under UV-light irradiation (λ = 275 nm) with characteristic Eu^{III} and Tb^{III} emission spectra displayed for the Eu-gel and Tb-gel, respectively. Mechanically mixing equal volumes of the two gels resulted in a new yellow-orange luminescent gel which showed two main emission bands occurring at 545 nm and 616 nm, corresponding to coordinates of (0.47, 0.47) on a CIE diagram. Morphology studies by SEM showed that both the Eu-gel and Tb-gel have a "cotton-like" fibrous microstructure but with different porosity; the Tb-gel exhibiting higher density of fibre packing; while the mixed gel had different morphological features to the "pure" gels. Furthermore, these gels showed self-healing characteristics by 'the naked-eye' and by rheology studies.

Acyclic btp ligands **51** and **52** are another class of tridentate coordinating ligands which have recently been implemented for both Ln^{III} sensitization and healable soft-material generation in our laboratory.[80] Precursor **51** was shown to form the three expected assemblies in solution - the 1:1, the 1:2 and the 1:3 (Eu:**L**) stoichiometric species (with binding constants of $\log_{\beta 11} = 8.4$, $\log_{\beta 12} = 16.2$ and $\log_{\beta 13} = 22.3$ calculated), following the addition of $Eu(CF_3SO_3)_3$ to a solution of **51** in CH_3CN. Crystals of the solid state Eu.$\mathbf{51}_3$ complex were grown and revealed a fully saturated Ln^{III} coordination sphere, see Figure 7. The LMWG tricarboxylic acid derivative **52** was employed for the formation of hydrogel and metallogel materials with the incorporation of the acid 'bridging

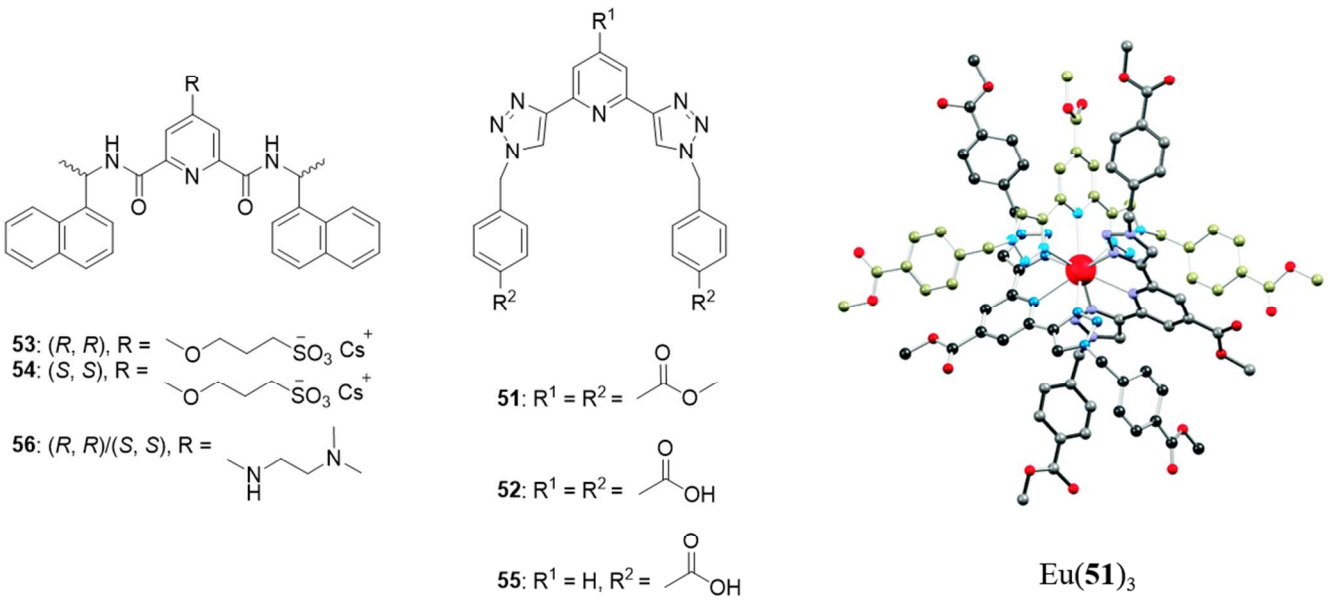

Figure 7. 'Trinity Sliotar' analogues **53**, **54** and **56**, btp ligands **51**, **52** and **55** and X-ray crystal structure of Eu(**51**)$_3$ (Reproduced from ref. 80 with permission from The Royal Society of Chemistry).

points' facilitating hydrogel formation of **52** *via* hydrogen bonding interactions. The hydrogel was characterized by TGA, rheology and SEM studies which displayed a tightly packed fibrous network of intertwined 'spaghetti-like' strands (*ca* 20-50 nm in diameter). The metallogel was synthesized by adding 3 equiv. of Eu(OAc)$_3$ to a solution of the Eu.**52**$_3$ complex and reacting under microwave radiation at 80 ^{o}C for 30 mins, after which an off-white soft precipitate was observed upon cooling. A highly robust gel resulted, which displayed the characteristic red Eu^{III}-centred emission under UV lamp excitation, while lifetime studies confirmed the presence of two different Eu^{III} environments - one located in the original Eu.**52**$_3$ complex and the second acting as a bridging centre between adjacent complexes. SEM imaging elucidated a different morpology to that seen for the hydrogel while rheology studies confirmed the significant self-healing property of the metallogel. This study highlights the ability of the Ln^{III} centre to not only act as a cross-linker in the 3D network but to impart physical characteristics on the overall structure.

Since H_2O is the most abundant solvent in nature designing scaffolds for the construction of responsive supramolecular entities in an aqueous environment is hugely important. For the purpose of applying the function of such systems to use in 'real-life' situations, (be it the monitoring of biological/environmental species or the generation of biomimetic systems), water solubility is critical. Water solubility of the aforementioned 'Trinity Sliotar' system has recently been accomplished by grafting a sulfonate motif to the 4-pyridyl position of **36** and **37**, yielding chiral analogues **53** and **54**.[117] Again, binding constants of the various stoichiometric species assembled in solution upon Eu^{III}-directed assembly ($\log_{\beta 11}$ = 7.4, $\log_{\beta 12}$ = 12.2 and $\log_{\beta 13}$ = 19.1 for the Ln.**54**, Ln.**54**$_2$ and Ln.**54**$_3$ species respectively - obtained from UV-visible absorption H_2O studies) and quantum yields (12%) were calculated from photophysical measurements which were conducted in a 100% H_2O solution. The binding affinity of the self-assembly process was also quantified using the chiroptical changes of the system by fitting the changes in the CD spectra. Results calculated from this technique compared well to those calculated from ground and excited state measurements. Moreover, hydrogels of both ligands were formed, upon heating in the presence of Cs_2CO_3, which were stable to the inversion test. SEM imaging displayed a smooth gel surface with networks of layered material consisting of more complex fibrous networks underneath. Addition of Eu^{III} to these hydrogels initially generated a red luminescent metallogel; however, upon aging were shown to be unstable, undergoing a phase transition from gel to sol. An extension to this work has been the development of a molecular logic gate mimic in which two responsive emissive complexes (a green luminescent 1:3 Tb-btp complex (Tb.**55**$_3$) and a red luminescent 1:3 Eu-dpa complex (Eu.**56**$_3$)) have been non-covalently incorporated within a p(HEMA-co-MMA) polymer organogel and shown to be dually responsive to the inputs [H+] and [F-]. Upon acidification of the system, Eu^{III} emission from the Eu.**56**$_3$ complex within the gel was enhanced, while Tb^{III} emission from Tb.**55**$_3$ was concomitantly quenched (*ca.* 80%), with a minor enhancement observed in the ligand fluorescence band of **55**, centred at 338 nm. However, fluoridation resulted in a complete 'switching–off' of the Eu^{III} centred emission, with a decrease in Tb^{III} centred emission (*ca.* 80%) and a 3 fold enhancement in ligand fluorescence. Fluoridation followed by acidification gave rise to a Eu^{III} centred emission enhancement with a simultaneous decrease in the Tb^{III} emission and an increase in fluorescence (greater than that observed following just acidification alone). This resulted in four distinguishable output states (*i.e.* luminescence profiles) which were shown to mimick three parallel logic gates in a double-input-three-output logic circuit - one of only a few examples to date of the use of the Ln^{III} as outputs in molecular logic [118]

Clearly strides to establish these simple building blocks as potential candidates for nanotechnological purposes have been made in recent times with future advances promising to be fruitful.

Another example, not strictly a mononuclear Ln^{III}-directed system, but worth discussing at this point nonetheless, from a soft materials perspective, is the luminescent Eu^{III} –based hydrogel formed from the tripodal terpyridine-based LMWG ligand **57**. Spectroscopic techniques were employed to probe the self-assembly behaviour of **57** with Eu^{III} ($Eu(CF_3SO_3)_3$, $EuCl_3$ and $Eu(NO_3)_3$ salts were investigated) and to elucidate the binding constants of the various stoichiometries formed in solution – the assembly of the 1:1 and 3:2 (Ln:**57**) species were observed with binding constants of $\log_{\beta 11} = 7.3$ and $\log_{\beta 32} = 24.9$ calculated for the titration with $EuCl_3$ in CH_3OH.[119] H_2O:CH_3OH solvent mixtures of 70:30 and 5:95 were then employed for the gelation process, giving rise to the formation of transparent supramolecular gels of **57** and $EuCl_3$.**57**, respectively. Thermogravimetric analysis (TGA), ^{1}H NMR and mass spectrometry confirmed an initial preorganization of the terpy ligand into supramolecular helices - organised by threefold H-bonding and π-π stacking; while SEM, TEM and energy-dispersive X-ray spectroscopy suggested that the Eu^{III} was then acting as a supramolecular 'glue', giving a more ordered gel with higher stability, by intermolecularly connecting the **57** polymer structures through coordination to terpy units on adjacent strands.

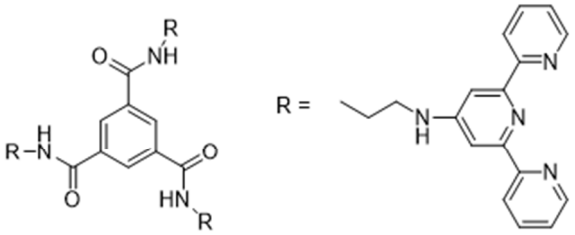

57

These metallogels also displayed a retention of the luminescent properties of the Eu-terpy assembled units within the gel matrix. An intriguing aspect of this study was the growth of salt nanowires at the surface of the supramolecular gels. SEM, TEM and energy-dispersive X-ray spectroscopy (EDX) elucidated that micrometre-scale euhedral-like sodium chloride crystals formed at the gel matrix surface, *via* diffusion-driven base growth, following 3-4 days aging at ambient conditions. This is the first example of the use of such supramolecular gels to grow chemical nano-gardens of common halide salts.[120] More recently, supramolecular gels of **57** have also been cross-linked into 3D networks with a range of *d*-block metals such as Fe^{II}, Ni^{II}, Cu^{II}, Zn^{II} and Ru^{II}, highlighting the versatility this system has to offer.[121] Compound **57** has also recently been implemented by Jung and co-workers for the formation of a ''turn-on'' aggregation-induced emission (AIE) fluorescent chemoprobe for Zn^{2+}.[122] This research group has also employed ligand **57**, along with novel chiral components, to generate helically templated gold nanoparticle superstructures. [123]

3 Multimetallic self-assembly structures from acyclic ligands

On account of the lability and relatively unpredictable nature of the Ln^{III} coordination preferences the construction of discrete synthetically controlled polymetallic Ln^{III} containing architectures can prove quite a challenge to the supramolecular chemist. Nonetheless, by manipulating ligand design for pre-organization the variable coordination numbers and stereochemical inclination of the Ln^{III} may be accommodated for - which is reflected by the growing number and diverse range of emerging multimetallic Ln^{III}-directed superstructures, such as cages, clusters, grids, helicates, MOF's and interlocked structures, in recent times. A brief overview of a select few examples of these assemblies is discussed.

3.1 Clusters, cages and grids

As mentioned, Ln^{III} based chiral supramolecular architectures are attractive for chiral sensing purposes. In view of this the chiral carboxylate-derivatised bipyoxazoline tetradentate ligand **58** was synthesized for use in the diastereoselective self-assembly synthesis of an enantiopure trinuclear Eu^{III} cluster complex *via* a concentration-dependent process. The evolution of the diastereomeric self-assemblies (Δ)-$[Eu(\mathbf{58})_2]^+$ and (Λ)-$[Eu(\mathbf{58})_2]^+$ were formed with partial stereoselectivity ($\Lambda/\Delta \approx 1.8$) at low concentrations while at higher concentrations selective homochiral recognition affords the trinuclear $[(\Delta\Delta\Delta)\text{-}Eu(\mathbf{58})_2)_3]^{3+}$ triangular complex exclusively, see Figure 8.[49] Moreover, Mazzanti *et al.* have further enhanced the controlled complexity of these systems by synthesizing the enantiomer **59** and assembled, by the addition of Eu^{III} to a mixture of diastereoisomers of either the bis ligand **58** complex or the bis ligand **59** complex, large multimetallic enantiopure wheels.[124] The addition of Eu^{III} to a mixture of (Δ)-$[Eu(\mathbf{59})_2]^+$ and (Λ)-$[Eu(\mathbf{59})_2]^+$ gives rise to the selective self-assembly of the enantiopure heptameric Eu^{III} wheel $[Eu\subset(\Lambda\text{-}Eu(\mathbf{59})_2\Delta\text{-}Eu(\mathbf{59})_2)_3(CF_3SO_3)_9]$, see Figure 8, while the addition of Eu^{III} to a mixture of (Δ)-$[Eu(\mathbf{58})_2]^+$ and (Λ)-$[Eu(\mathbf{58})_2]^+$ yields the corresponding enantiomeric heptameric Eu^{III} $[Eu\subset(\Delta\text{-}Eu(\mathbf{58})_2\Lambda\text{-}Eu(\mathbf{58})_2)_3(CF_3SO_3)_9]$ ring. Both structures were elucidated by solid state X-ray crystallography and were shown to be isostructural while Eu^{III}-centred CPL emission was detected from the mononuclear, trimeric and heptanuclear species. Of these, the trimeric complexes showed remarkable CPL activity in comparison to the mono- and heptanuclear species with g_{lum} values (for the $^5D_0 \rightarrow {}^7F_1$ transition) of -0.04 and +0.06 (for the mononuclear species), ±0.45 (for the trimeric species) and +0.1 (for the heptameric species) obtained.

The first Ln^{III} containing tetrahedral assembly was reported by Hamacek in 2008.[125] Using the diamido pyridine motif as the tridentate chelating unit and a short spacer, tripodal ligand **60A** was shown, by NMR, ESI-MS and spectrophotometric solution studies, to assemble *via* Ln^{III}-directed coordination forming discrete 3D tetrahedral assemblies $[Ln_4\mathbf{L}_4]^{12+}$ (Ln = Eu^{III}, Lu^{III} and Tb^{III}). Species with different stoichiometries were also observed, by ESI-

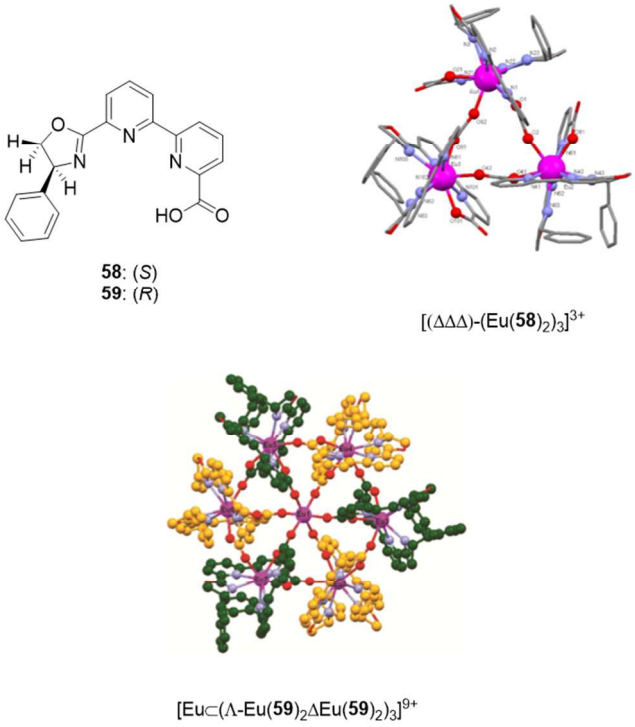

Figure 8. Compounds **58** and **59** designed for the formation of the trimeric $[(\Delta\Delta\Delta)\text{-}Eu(\mathbf{58})_2)_3]^{3+}$ and heptanuclear $[Eu\subset(\Lambda\text{-}Eu(\mathbf{59})_2\Delta\text{-}Eu(\mathbf{59})_2)_3]^{9+}$ self-assembly cluster structures. Reprinted with permission from ref. 124. Copyright (2012) American Chemical Society.

MS and spectrophotometric measurements, when either the ligand/metal were in excess, however, binding constant values, elucidated from UV-visible measurements ($\log\beta_{4,4}$ = 39.7) confirmed formation of the tetrahedral complex as the major species. Crystals of the $[Tb_4\mathbf{60A}_4]^{12+}$ complex were grown and showed the predicted structure of the complex with the four metal ions occupying the vertices of the tetrahedral cage, each coordinated to three different ligands, while the face of the tetrahedron is occupied by the ligand.

In depth analysis of the thermodynamics of the self-assembly process between **60A** and a number of Ln^{III} metal ions (Ln = La^{III}, Nd^{III}, Eu^{III}, Tb^{III}, Er^{III}, Lu^{III}) in CH_3CN have also been conducted, again illustrating that by simply altering the metal/ligand ratio the formation of other species can be generated. Notable from this study was the assembly of the trinuclear $[Lu_3\mathbf{60A}_2]^{9+}$ complex which was assembled in the presence of excess metal and characterized by X-ray crystallography, displaying two inequivalent ligands with one adopting an *endo*-CH_3 and the other adopting an *exo*-CH_3 conformation.[126]

Further studies on this system involved the replacement of the amide linker with an ester group, yielding tripodal tris(tridentate) ligand **61** and, following self-assembly, subsequent tetrametallic cage $[Ln_4\mathbf{L}_4]^{12+}$ (Ln^{III} = La^{III}, Eu^{III}, Lu^{III}) formation.[127] Modification at this position provided a larger cavity size capable of accommodating guest anions, unlike that seen for $[Tb_4\mathbf{60A}_4]^{12+}$, which was evidenced by the X-ray crystal structure of $[Eu_4\mathbf{61}_4](OH)(ClO_4)_{11}$, see Figure 9, where all anchoring methyl groups direct out of the tetrahedron centre (*exo*-CH_3), contrary to

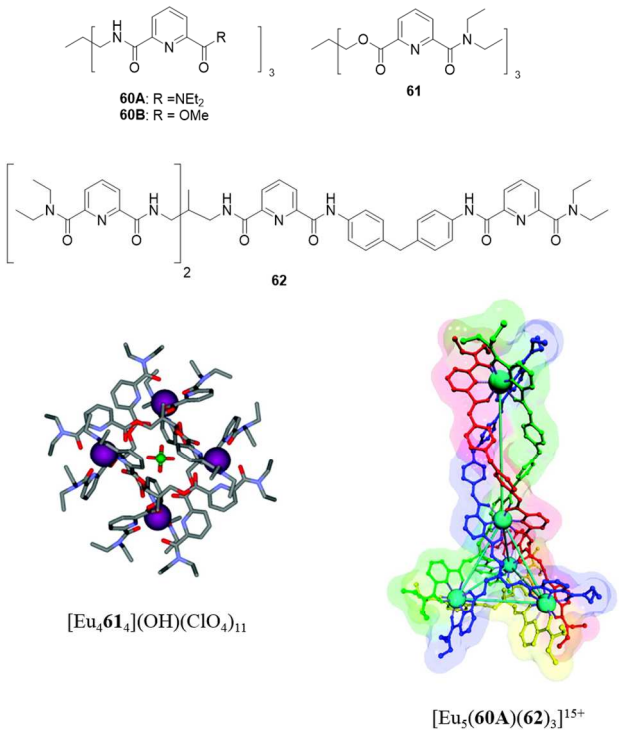

Figure 9. Compounds **60A** – **61**, X-ray crystal structure of $Eu_4\mathbf{61}_4(OH)(ClO_4)_{11}$ (hydrogen atoms, uncoordinated anions and solvent molecules are omitted for clarity) and pentanuclear Ln^{III} helicate $[Eu_5(\mathbf{60A})(\mathbf{62}))_3]^{15+}$ (molecular model shown). Reprinted with permission from ref. 127 and 130. Copyright (2011) American Chemical Society.

$[Tb_4\mathbf{60A}_4]^{12+}$ (*endo*-CH_3), generating an expanded volume. Host-guest exchange interactions were investigated using NMR techniques revealing the ability to exchange an initially localized perchlorate anion with small anion guests such as BF_4^-, Im^- and I^-; however competition with direct Ln^{III} coordination and subsequent cage destruction was an issue with other anions. More recently a triptycene moiety has been utilized as a spacer unit in such systems to increase the distance between the metal ions and provide an even larger cavity volume.[128] Ligand **60B** has also been designed for the construction of tetranuclear tetrahedral cages with the formation of such edifices preferentially forming with the heavier Ln (Ln = Tb^{III}, Er^{III}, Lu^{III}).[129]

The importance of ligand pre-programming for the construction of pre-determined higher order molecular edifices has been markedly emphasised in a rather impressive extension to this work. The self-assembly of the first pentanuclear Ln^{III} helicate has been driven by metal coordination of one symmetric tridentate ligand **60A** and three unsymmetric tripodal tetradentate ligands **62** to five Ln^{III} metal ions.[130] As shown, **60A** forms the tetrahedron base while the three **62** ligands form the side faces and linear part of the supramolecular structure. By precisely combining previously studied chemical motifs (in a 5:1:3 Eu:**60A**:**62** ratio) the assembly of $[Eu_5(\mathbf{60A})(\mathbf{62})_3]^{15+}$ (MM2 shown in Figure 9) was achieved and verified by NMR and ESMS studies, demonstrating the successful application of pre-disposition for controlled synthesis of Ln^{III} containing

multinuclear assemblies.

Cerium based tetrahedron cages which employ ligands **63** and **64** have been developed by Duan and co-workers for the size-selectively sensing of carbohydrates.[131] Both **63** and **64** possess two tridentate pre-organized motifs available for metal ion coordination and subsequent tetrahedron formation. Evaporation of CH_3OH-DMF solutions of ligands **63** and **64** with $Ce(NO_3)_3.6H_2O$ in air for several days led to the formation of crystalline solids of Ce_4**63**$_6$ and Ce_4**64**$_6$, respectively, which showed the four metal centres at each corner, each coordinated to three tridentate chelating groups in a coronary triangular prism coordination geometry. The sensitivity of the luminescence band centred at 525 nm, which is attributed to the $5d \rightarrow 4f$ transition of Ce^{3+}, was exploited as a signalling unit where a considerable luminescence intensity enhancement was experienced with increasing concentration of hexoses; however only small intensity variations (10%) were observed following the addition of pentoses, such as ribose or xylose to Ce_4**63**$_6$, while no obvious changes were observed when disaccharides were added, suggesting the possible size-selective recognition of Ce_4**63**$_6$ toward the hexoses over the smaller pentose and disaccharides studied.

Coordination cages of this nature have also been employed as 'molecular flasks' prompting the cyanosilyation of aromatic aldehydes within their cavity.[131,132] Tripodal ligands **65** – **67** were designed such that the distance between the three chelating groups was tailored to dictate the overall size of the internal cavity. By size-selectively forcing substrates into close proximity the cages exhibited enzymatical catalytic activity while simultaneously 'reporting' the concentration of the guest by an optical output.

Chiral bis(tridentate) and tris(tridentate) ligands **68** and **69** have been designed by Bünzli and co-workers for the assembly of edge and face-capped self-sorting luminescent Eu^{III} tetrahedral cages.[131,133] The pyridine-2,6-dicarboxamide chelating unit coordinates to four metal atoms at the vertices of the tetrahedron, yielding Eu_4(**68**)$_6$ and Eu_4(**69**)$_4$, in the case of **68** and **69** respectively, where the bidentate ligands occupy the edges of Eu_4(**68**)$_6$ and the tridentate ligands are mapped to each of the faces of the tetrahedron of Eu_4(**69**)$_4$. Stereoselective homochiral formation of ΔΔΔΔ and ΛΛΛΛ complexes was induced by ligand chirality and confirmed by X-ray crystallography, circular dichroism and NMR enantiomeric differentiation experiments. Furthermore, when an equimolar mixture of **68** and **69** was assembled in solution with Eu^{III} the individual tetrahedron cages Eu_4(**68**)$_6$ and Eu_4(**69**)$_4$ were synthesized, described as "narcissistic" self-sorting behaviour, where the self-assembly process discriminates between differently shaped ligands **68** and **69**. In addition to this self-sorting behaviour, reaction of Eu^{III} with an equimolar mixture of *R* and *S* enantiomers of **69** led to the formation of homoligand chiral cages ΔΔΔΔ-**69** and ΛΛΛΛ-**69** as a racemic mixture, as ascertained by ^{1}H NMR, DOSY and ESI-TOF-MS experiments. When Δ-TRISPHAT (6 equiv.) was added to the racemic mixture distinguishable diastereomeric signals were observed in the ^{1}H NMR spectrum, further confirming homoligand cage formation. In addition to this self-sorting crystallization also occurred after THF-vapour diffusion into the racemic mixture yielding single crystals possessing the same unit cell parameters, but opposite optical activities (measured by CD spectroscopy after redissolution). However, in the case of **68** a dynamic mixture of scrambled-ligand cages, Eu_4(**68**^{R})$_4$(**68**^{S})$_{6-n}$ (n = 0-6) were formed.

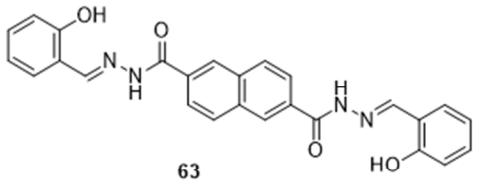

63

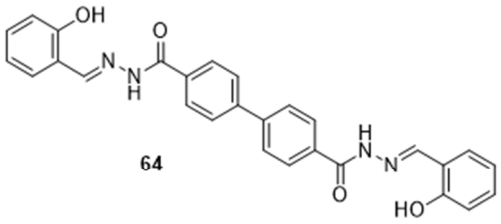

64

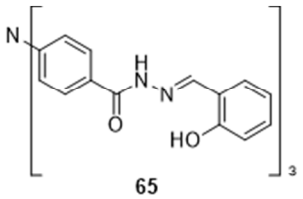

65

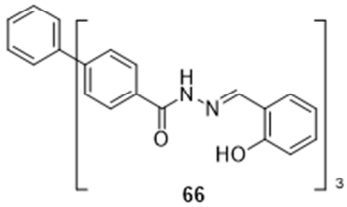

66

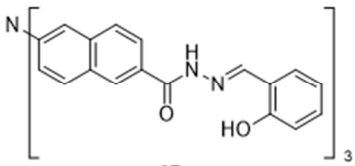

67

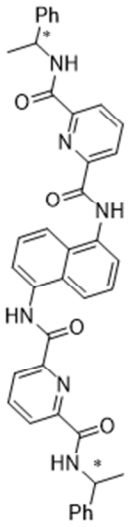

68

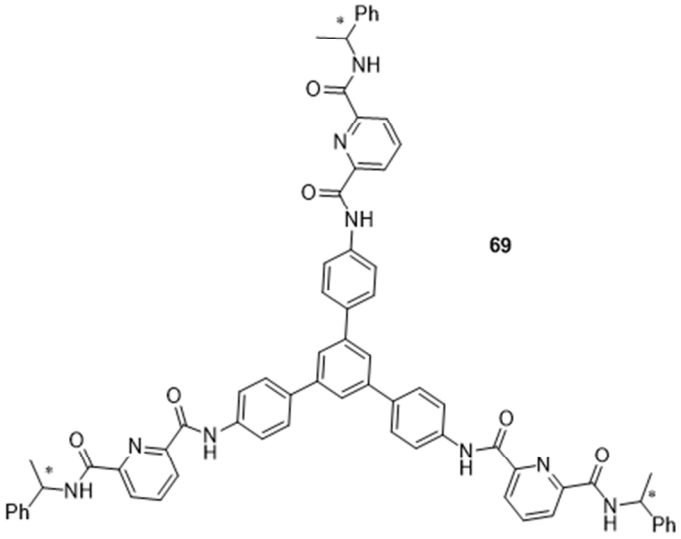

69

Tris(tridentate) pyridinebis(hydrazone)-based ligands **70** and **71** have proven to be competent candidates in the direction of first row transition metal ion [2 x 2] and [3 x 3] grids.[134-136] Following these findings it was anticipated, by Thompson and co-workers that coordination of **70** and **71** with the Ln^{III} may also lead to grid formation. However, initial studies resulted in the formation of a Gd^{III} mononuclear (1:1, Gd:**L**) structure and linear trinuclear (3:2) (Ln:**L**, Ln = Gd^{III}, La^{III}, Dy^{III}) structures with **70** and **71**, respectively.[137] The Gd^{III} ion was shown, by X-ray crystallography, to occupy the tridentate NO_2 binding pocket of **70** only, in the mononuclear structure, with two bidentate nitrates and two *N*,*N*-dimethylformamide molecules completing the metal coordination sphere. In the trinuclear complexes each Ln^{III} ion was shown to occupy two N^N^O and one O^N^O tridentate binding pocket of two coordinating ligands **71**. Four hydrazone μ-O atoms

bridge the three metal centres in a helical linear fashion while benzoate, nitrate and *N*,*N*-dimethylformamide coligands complete their coordination spheres. A significant observation was the exhibition of single-molecule magnet behaviour in the Dy^{III}_3 trinuclear complex. Considering the flexibility of ligands **70** and **71** it was suggested that the trinuclear species was not attainable for **70** as a result of rotational restrictions. Bis(tridentate) carbohydrazone complexes of **72** were therefore synthesised, providing sufficient flexibility to appropriately organise the Ln^{III} ions into grids. The first three examples of square, heteroleptic self-assembled [2 x 2] Ln^{III}_4 grids were synthesised by reacting **72** with either $DyCl_3.6H_2O$ or $Tb(NO_3)_3.5H_2O$ in CH_3CN/CH_3OH in the absence or presence of NaN_3.[138] It was shown by X-ray crystallography that four Ln^{III} occupy two tridentate N_2O ligand pockets in four ligands, arranged in pairs above and below the planar, square core arrangement of four Dy^{III} and Tb^{III} ions giving complexes $[Dy_4(\mathbf{72}\text{-}2H)_2(\mathbf{72}\text{-}H)_2(OH)_4]Cl_2\cdot 8H_2O$, $[Dy_4(\mathbf{72}\text{-}2H)_2(\mathbf{72}\text{-}H)_2(N_3)_4(O)]\cdot 14H_2O$ and $[Tb_4(\mathbf{72}\text{-}2H)(\mathbf{72}\text{-}H)_3(N_3)_4(O)](NO_3)(CH_3CN)\cdot 2H_2O$.

Four exogenous μ-OH bridges link the Dy^{III} ions within $[Dy_4(\mathbf{72}\text{-}2H)_2(\mathbf{72}\text{-}H)_2(OH)_4]Cl_2\cdot 8H_2O$ whereas μ_2-1, 1-N_3^- bridges replace these OH bridges in $[Dy_4(\mathbf{72}\text{-}2H)_2(\mathbf{72}\text{-}H)_2(N_3)_4(O)]\cdot 14H_2O$ and $[Tb_4(\mathbf{72}\text{-}2H)(\mathbf{72}\text{-}H)_3(N_3)_4(O)](NO_3)(CH_3CN)\cdot 2H_2O$ with a μ_4-O (oxide) ion occupying the central position within the square, bridging all four Dy^{III} ions, as shown for $[Dy_4(\mathbf{72}\text{-}2H)_2(\mathbf{72}\text{-}H)_2(N_3)_4(O)]\cdot 14H_2O$ in Figure 10. Exhibition of SMM behaviour was displayed by $[Dy_4(\mathbf{72}\text{-}2H)_2(\mathbf{72}\text{-}H)_2(N_3)_4(O)]\cdot 14H_2O$ but not by $[Dy_4(\mathbf{72}\text{-}2H)_2(\mathbf{72}\text{-}H)_2(OH)_4]Cl_2\cdot 8H_2O$, suggesting that the azide bridges may play an important role in the magnetic properties of the Dy^{III}_4 [2 x 2] grid. The scope of this project was further extended to include other Ln^{III} (Ln^{III} = Gd^{III}, Dy^{III}, Ho^{III}, Yb^{III} and Eu^{III})

with derivatives of the carbohydrazone ligand **72** in the development of novel self-assembled [2 x 2] grids.[139,140]

Tang and co-workers have also employed pyridinebis(hydrazone)-type ligands for the assembly of 4*f*-4*f* and 4*f*-3*d* grids.[141] By reacting **73** with either $DyCl_3 \cdot 6H_2O$ or $Dy(CF_3SO_3)_3 \cdot 6H_2O$ in 1:2 CH_3OH/CH_3CN colourless crystals of the 4*f*-4*f* grids $[Dy_4(\mathbf{73})_4Cl_4(H_2O)_8] \cdot Cl_8$ and $[Dy_4(\mathbf{73}\text{-}2H)_4(H_2O)_{12}] \cdot (CF_3SO_3)_4 \cdot 12H_2O$, respectively, were grown. In both cases the four ligands were shown to occupy the edges of the square grids with the four metal ions residing at each corner, each Dy^{III} coordinated to two tridentate N_2O binding moieties on two different ligands. In the case of $[Dy_4(\mathbf{73}\text{-}2H)_4(H_2O)_{12}] \cdot (CF_3SO_3)_4 \cdot 12H_2O$ the Dy^{III} coordinating geometry is completed by three water molecules, meanwhile, for $[Dy_4(\mathbf{73})_4Cl_4(H_2O)_8] \cdot Cl_8$, the coordination sphere is completed by two water molecules and one Cl^-. The novel dihydrazone ligand **74** was also designed for grid construction, possessing two larger O^N^N^O binding pockets for 4*f* coordination and one

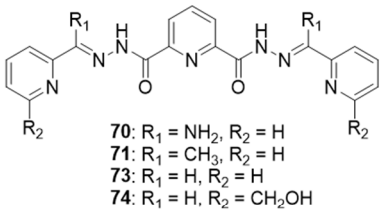

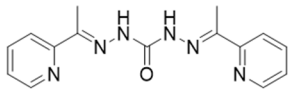

72

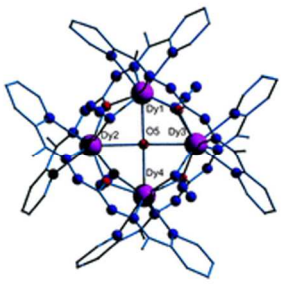

$[Dy_4(\mathbf{72}\text{-}2H)_2(\mathbf{72}\text{-}H)_2(N_3)_4(O)] \cdot 14H_2O$

Figure 10. Cluster ligands **70** – **74** and X-ray crystal structure of $[Dy_4(\mathbf{72}\text{-}2H)_2(\mathbf{72}\text{-}H)_2(N_3)_4(O)] \cdot 14H_2O$ (reproduced from ref. 138 with permission from The Royal Society of Chemistry).

smaller N_3 binding pocket for 3*d* coordination. Upon reacting **74** with $DyCl_3 \cdot 6H_2O$ and $CuCl_2 \cdot 2H_2O$ in the presence of NEt_3 crystals of the 4*f*-3*d* grid $[Dy_4Cu_4(\mathbf{74}\text{-}2H)_4Cl_8(H_2O)_4].Cl_4 \cdot 28H_2O$ were grown. Similarly to the 4*f*-4*f* grids of ligand **73** above the four ligands were shown to occupy the edges of the square grids while the four metal ions were coordinated to two tetradentate O^N^N^O binding moieties of two different ligands at the corners; with one H_2O molecule completing the coordination sphere of each Dy^{III}. Four N_3 binding pockets along the squares edges provide a tridentate coordinating unit for each of the four Cu^{II} ions, giving an overall square shaped 4*f*-3*d* grid structure. Magnetic susceptibility measurements were also performed on the above three complexes with the 4*f*-3*d* grid displaying the most promising SMM behaviour, representing the first 4*f*-3*d* grid exhibiting such a feature.

Ln^{III}-containing (poly)metallic cluster compounds, (Dy^{III} clusters in particular), display fascinating magnetic behaviour and have therefore received considerable attention for the purpose of constructing novel single-molecule magnet-based devices as these systems have possible applications in high-density information storage, quantum computing and spintronics. For more in-depth articles on this topic one is directed towards more relevant references, focusing more intently on the magnetics of Ln^{III} containing cluster compounds.[142-149]

3.2 Helicates

Following on from leading researchers in the field of helicate supramolecular chemistry, such as Lehn, Savage and Constable, [150-155] Bünzli and Piguet have paved the way further, laying down foundations in the development of novel multimetallic Ln^{III} luminescent helicate structures Pioneering work has primarily been based on the bis(benzimidazole)pyridine framework which has been intensely studied as a precursor for Ln^{III}-driven coordination, sensitization and higher order helicate assembly.

Over the past 20 years or so many analogues of the original bis(benzimidazole)pyridine system have been developed and progressively altered in order to adjust the system and enhance both the structural and photophysical properties for eventual biological/materials based application purposes; and to better understand the thermodynamics of the self-assembly process itself. This work has been reviewed by us and others previously, [23,156,157] however, a brief overview is essential given the advancements that have been made and the impact it has had on this discipline.

Study of the bis(benzimidazole)pyridine platform as a helicate precursor seems to have originated from a publication in the early 1990s by Piguet and co-workers. in which a bis(bidentate) bis(l-methyl-2-(6'-methyl-2'-pyridyl)benzimida-zol-5-yl)methane ligand formed a bimetallic triple helical complex upon self-assembly with Co^{II}.[158] Since then, the bis(benzimidazole)pyridine unit has undergone tremendous study for the incorporation of the luminescent Ln^{III} ions. Initially, the bis(benzimidazole)pyridine scaffold was functionalized by an additional two terminal benzimidazole units, affording the symmetric ligand **75**, which is pre-organized such that two tridentate units are well defined, and separated by a flexible -CH_2 spacer. An X-ray crystal structure of the first self-assembled binuclear triple-helical Ln^{III} complex $[Eu_2(\mathbf{75})_3](ClO_4)_6 \cdot 9CH_3CN$, as shown in Figure 11, shows **75** wrapped around a helical axis defined by two Eu^{III} ions with aromatic stacking between the three ligand strands. In each coordination sphere the Eu^{III} is nine-coordinated by the six nitrogen atoms of the benzimidazole units and the three nitrogen atoms of the pyridine groups, respectively This gives a structure with a slightly distorted tricapped trigonal prismatic geometry; confirming the formation of the triple stranded bimetallic

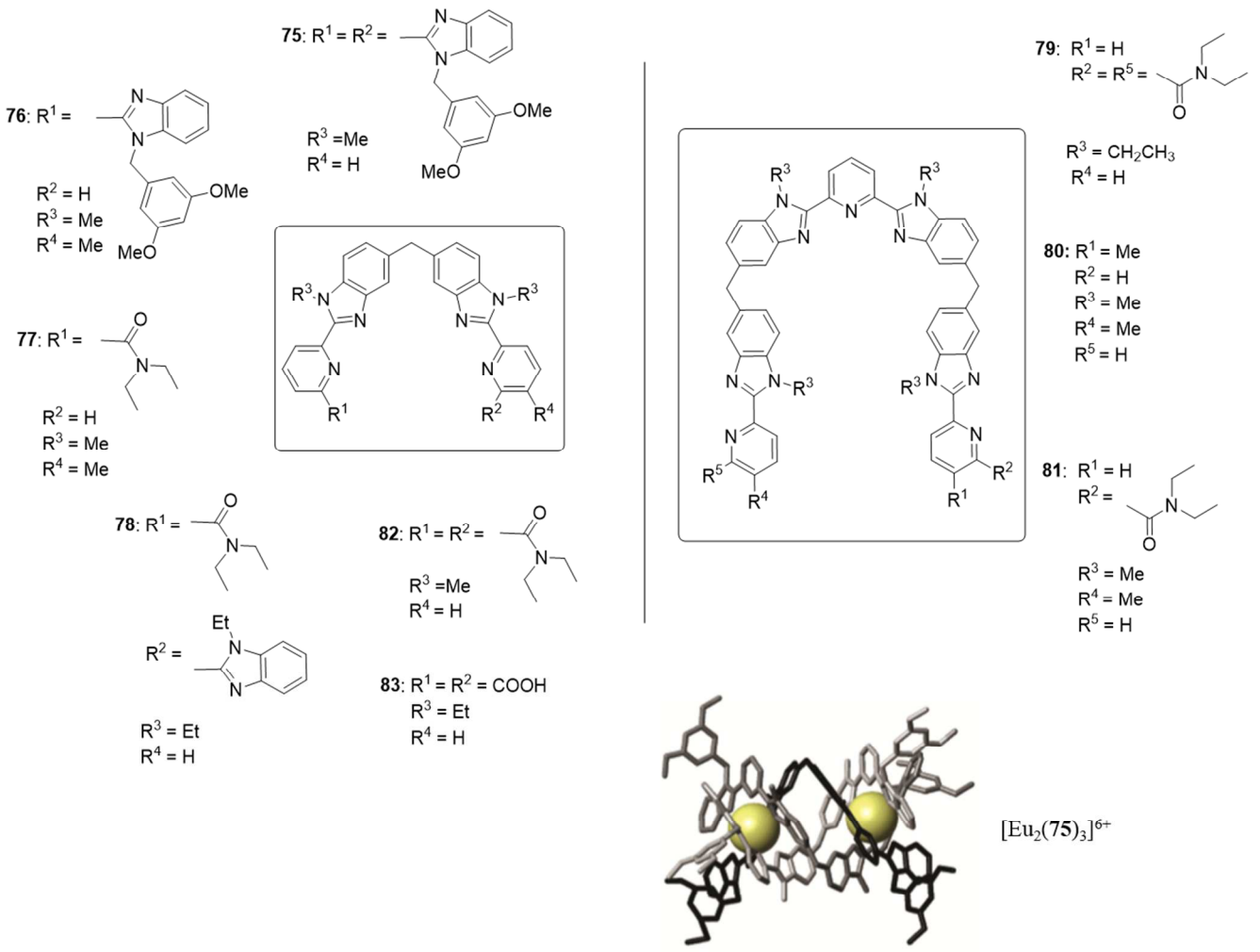

Figure 11. Bis(benzimidazole)pyridine compounds **75** – **83** for the formation of bimetallic triple stranded helical complexes and X-ray crystal structure of $[Eu_2(\mathbf{75})_3]$. Reprinted with permission from ref. 161. Copyright (2003) American Chemical Society.

helicate.[159] A drawback was the quenching of the Ln^{III}-centred luminescence, however, as the ligand strands were not sufficiently "rigid enough" to fully protect the metal centre from interacting with solvent/anion molecules in the surrounding environment.[160] The formation mechanism of this supramolecular system was studied in great detail with three major species characterised in CH_3CN solution ($\log\beta_{12} = 11.6$, $\log\beta_{22} = 18.1$ and $\log\beta_{23} = 24.3$ for $Eu\mathbf{75}_2$, $Eu_2\mathbf{75}_2$ and $Eu_2\mathbf{75}_3$, respectively). This study also indicated that the self-assembly process was mainly governed by electrostatic interactions between the ligands and the Eu^{III}. Supramolecular devices expressing dual functionality opens up new opportunities for the development of multi-responsive probes. In light of this, the inclusion of two or more different *d*- or *f*- block metal ions into heteropolymetallic triple stranded helicates has received appreciable attention where ligand **76** was synthesized for the self-assembly of the first *d-f* heterobinuclear triple helix in solution.[162] Grafting *N,N*-diethylcarboxamido groups in place of the benzimidazole group led not only to an increase in both selectivity and Ln^{III}-centred luminescence quantum yield but replacement of the benzimidazole group with a *N,N*-diethylcarboxamido group resulted in a crystalline material that was suitable for X-ray crystallographic analysis in the case of $[EuZn(\mathbf{77})]^{5+}$; which was the first luminescent self-assembled helical *d-f* complex to be structurally characterised.[163]

Significant effort to pre-programme helicate ligands for the selective recognition and self-assembly of *f-f* heterobimetallic triple stranded helicates, based on Ln^{III} size discrimination, has also been made. By implementing the ditopic ligand **78**, which bears a benzimidazole-pyridine-carboxamide tridentate moiety, coded to preferentially coordinate smaller Ln^{III} and a less strongly coordinating bis(benzimidazole)pyridine unit, which preferentially binds larger Ln^{III} ions, X-ray crystal structures of a number of heterobimetallic species were grown and evaluated confirming structural data obtained from solution studies - representing the first unsymmetric ditopic ligand pre-organized to selectively bind heteropairs of Ln^{III} based on the difference in their ionic radii.[164,165]

An extension of the bis(benzimidazole)pyridine backbone to integrate three tridentate binding units led to the development of symmetric tritopic ligand **79**. The X-ray crystal structure of the homonuclear $[Eu_3(\mathbf{79})_3](CF_3SO_3)_9(CH_3CN)_9(H_2O)_2$ complex was obtained, displaying again the three ligand strands wrapping around each metal ion in a pseudo-threefold axis with each Ln^{III}

coordinated by nine donor atoms, giving rise to a pseudo-trigonal prismatic arrangement. Interestingly, the terminal sites (EuN_6O_3) display differences in electronic properties compared to the central site (EuN_9) in that the presence a low lying LMCT state resulted in luminescence from the two terminal EuN_6O_3 sites only Furthermore, under stoichiometric conditions, **79** was shown to assemble with different Ln^{III} to give a mixture of heterometallic triple stranded helicates in CH_3CN $[(Ln)_x(Ln')_{3-x}(\mathbf{79})_3]^{9+}$ with both coordinating sites (N_6O_3 and N_9) exhibiting different affinities for each specific Ln^{III}, again illustrating the dependence of the self-assembly process on the Ln^{III} size. Similarly to that corroborated above for **78**, the generally favoured heterotrimetallic helicate was that in which the central Ln^{III} site was preferentially occupied by the larger Ln^{III} with the two terminal N_6O_3 sites occupied by the smaller Ln^{III}.[166,167] By appending a fourth binding unit to the helicate backbone triple stranded tetranuclear heterometallic 4*f*-4*f* helicate systems of this type have also been developed.[168,169]

Derivatives of **76**, ligands **80** and **81** were synthesized for the formation of *d-f* heterotrinuclear triple helical structures.[170,171] As shown, ligand **80** possesses a tridentate central N_3 binding site connected to two terminal bidentate N_2 binding sites which is suitable for selective *d-f-d* block self-assembly formation of heterotrimetallic triple stranded helicates of the form $[MLnM(\mathbf{80})_3]^{7+}$ (M = Cr^{II}, Zn^{II}) and (Ln = La^{III}, Eu^{III}, Gd^{III}, Tb^{III}, Lu^{III}). For $[ZnLnZn(\mathbf{80})_3]^{9+}$ (Ln = Eu^{III}, Tb^{III}) Ln^{III}-centred luminescence was observed. However, in the case of $[CrLnCr(\mathbf{80})_3]^{9+}$ (Ln = Eu^{III}, Tb^{III}), Cr^{II} underwent rapid oxidation to Cr^{III}, resulting in the generation of non-emissive inert complexes. Compound **81** on the other hand, was designed with the intention of forming *d-f-f* metal ion self-assembly of heterotrimetallic triple stranded helicates for which the X-ray crystal structure of the $[ZnLu_2(\mathbf{81})_3]^{8+}$ complex was obtained.

Evidently, tremendous effort has been employed in order to extend and tailor the relatively simple bis(benzimidazole)pyridine core for the selective recognition of *d*- and *f*- block metal ions for subsequent formation of multifunctional heteropolymetallic triple stranded helicates. In conjunction with this an investigation into the applicability of water soluble Ln^{III} based homobimetallic helicates as biological sensors/imaging agents has been undertaken.[51,172-179] The helicate ligand analogue **82**, was found capable of forming highly stable bimetallic triple stranded helicates which were resistant to hydrolysis in moist CH_3CN up to 2.5 M H_2O.[180] These steps towards water stable Ln^{III}-directed helicate systems, led to the generation of **83**, which was responsible for the first lanthanide-containing helicate self-assembled in water.[181] Ligand **83** was shown to react with the entire Ln^{III} series forming neutral carboxylate homobinuclear triple stranded helicates of the form $[Ln_2(\mathbf{83}\text{-}2H)_3]$. These were found to be stable in water in the pH range of 4-13[182] while a competitive titration with 1,4,7,10-tetraazacyclododecane-*N,N',N'',N'''*-tetraacetic acid (dota) shows that the stability of the Eu^{III} helicate $[Eu_2(\mathbf{45}\text{-}2H)_3]$ is comparable to that of [Eu(dota)]. Furthermore, solid state X-ray crystallography of $[Ln_2(\mathbf{83}\text{-}2H)_3]$ complexes (Ln = Eu^{III}, Tb^{III}) confirmed the helicity of the three ligand strands wrapped around two nine-coordinate Ln^{III} to be of pseudo-D_3 symmetry.[183] Because of the high thermodynamic stability of the luminescent bimetallic triple stranded helicate $[Ln_2(\mathbf{83}\text{-}2H)_3]$ (Ln = Eu^{III}, Tb^{III}) in water, analogues of **83** were postulated as being ideal candidates for sensing/imaging capability studies in biological media.

Water solubility was even further enhanced by grafting a polyoxyethylene chain to the 4 pyridyl position, yielding **84**.[179] Ligand **84** was shown to exist as H_2L and HL- at physiological pH and, as was seen for **83**, formed thermodynamically stable neutral $[Ln_2(\mathbf{84})_3]$ complexes ($\log_{\beta 23}$ = 26 – 30 for Ln = La^{III}, Eu^{III}, Lu^{III}) upon self-assembly in TRIS-HCl buffered solution. The biological application of these structures were investigated in human cervical adenocarcinoma (HeLa) cells which were loaded with a 500 μM solution of $[Eu_2(\mathbf{84})_3]$ for 6 hrs., after which emission spectra and luminescence lifetime measurements confirmed cell permeation and also that the complex remained intact within the cells. Not only was staining of the cell cytoplasm achieved by permeation of $[Eu_2(\mathbf{84})_3]$ into the cells but cell viability after 24 hrs in the presence of $[Eu_2(\mathbf{84})_3]$ remained unaltered compared to cell viability in the absence of $[Eu_2(\mathbf{84})_3]$.

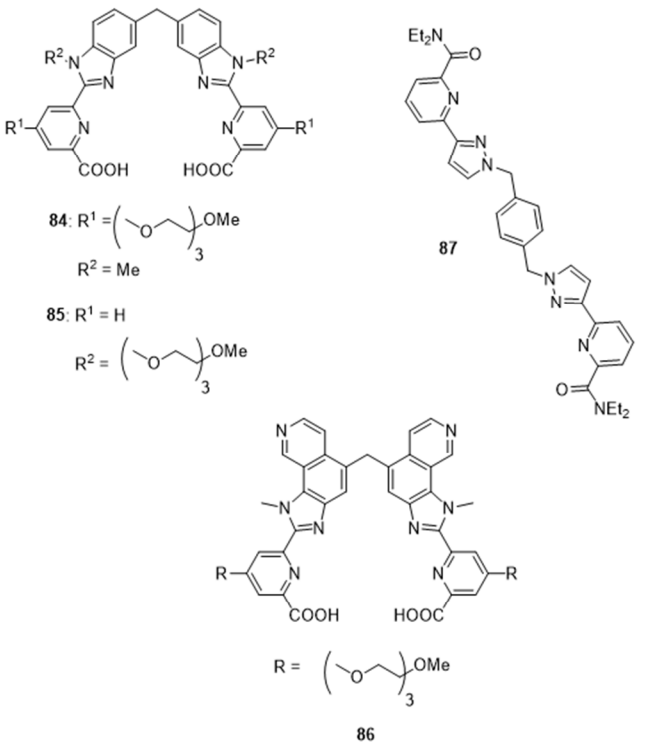

This indicated that the proliferation of the helicate complex into the HeLa cells had no noticeable influence on the health of the cells. Furthermore, $[Eu_2(\mathbf{84})_3]$ has also found use, in conjunction with acridine orange, as a pH insensitive luminescent probe for the analysis and quantification of DNA and PCR based products.[177] Derivatization of the initial ligand structure **83** with a polyoxyethylene group appended to both benzimidazole rings, afforded the related analogue **85**, where the water solubility was again enhanced and the formation in water of the highly stable neutral bimetallic triple stranded helicate $Eu_2(\mathbf{85})_3$ ($\log_{\beta 23}$ = 23.4) at physiological pH also allowed for the study of this complex as a cell staining agent. Luminescence microscopy detected Eu^{III}-centred emission from the cell cytoplasm at concentrations >50 μM after loading times of 20-30 mins. Again, the $Eu_2(\mathbf{85})_3$ complex remained intact following permeation *via* endocytosis

into the cell cytoplasm of several cancerous cell lines (MCF-7, HeLa, Jurkat and 5D10) while its effect on cell viability was estimated and concluded not to be significant. However, attachment of the polyoxyethylene chain to the benzimidazole ring did have an effect on the photophysics of the ligand excited state, resulting in a reduction in quantum yield from 18% to 11% for $Eu_2(\mathbf{84})_3$ and $Eu_2(\mathbf{85})_3$, respectively.[173,179,184] Unfortunately a drawback to the use of both $Eu_2(\mathbf{84})_3$ and $Eu_2(\mathbf{85})_3$ as biological luminescent tags was their short excitation wavelengths, which lie in the UV region at ~ 320 - 325 nm. Since it has been proven that substitution of the benzimidazole unit permits tuning of the photophysical properties of the resulting complex a series of compounds bearing different functional groups appended to the benzimidazole rings were developed, including ligand **86**, and the influence these different substituents have on the photophysical properties were then evaluated. The most promising results from this study were displayed by **86** where a compromise between the shifting of the excitation wavelength towards the visible range (330 nm → 365 nm) and a minimization of quantum yield decrease was achieved.[174] In an effort to further shift the excitation wavelength of these systems towards the visible and NIR range multiphoton-excitation has also been probed and proved successful as an alternative method.[175] More recently binuclear Ln^{III} luminescent helicates of this type have been bio-conjugated to avidin and tested for their specific recognition of a mucin-like protein receptor expressed on the surface of human breast cancer MCF-7 tumour cells.[51,176]

By systematically altering both the physical and chemical properties of earlier helicate ligands designed by Bünzli and Piguet *et al.,* these researchers have, in a stepwise manner, enabled their enhancement and employment in biological media. This novel class of luminescent compounds offers a number of distinctive advantages for implementation as imaging agents and as detection probes in bio-assays such as thermodynamic stability, kinetic inertness, appreciable luminescence quantum yields, long lifetimes, cell permeability, non-cytotoxicity, slow egression times and versatility for derivatization.

It is worth pointing out at this point that, for the past ten years or so, Piguet and co-workers has devoted much effort to describe the thermodynamic and kinetic aspects governing the self-assembly of multicomponent complexation processes. In order to predictably rationalize the formation of such supramolecular entities thermodynamic models have been developed, taking into account the various thermodynamic parameters responsible for complexation. This concept is outside the scope of this review however, and as such, will not be detailed here. Should the reader be interested, some relevant references are given.[185-189]

The above work highlights that elegant and exquisite superstructures are not solely the fruits of Ln^{III}-directed self-assembly but that by calculated ligand design and perseverance one may create and advance towards exciting new functional devices. For this reason this area of Ln^{III} encapsulation and property exploitation for the construction of higher order structures is currently a highly topical and fast growing area of interest with those such as Pikramenou *et al.,*[190] Albrecht *et al.*[47,48,191,192] and Faulkner *et al.*[193] applying their own strategies for the formation of Ln^{III} based helicate assemblies.

Faulkner *et al.* again makes use of the heterocyclic pyridine moiety in **87** in which two amide-pyridine-pyrazole tridentate binding pockets are connected through a phenyl spacer group for the formation of polynuclear coordination compounds. A range of architectures such as bimetallic triple stranded cylindrical mesocates $Ln_2(\mathbf{87})_3$ (Ln = Nd^{III}, La^{III}), bimetallic double stranded mesocates $Ln_2(\mathbf{87})_2$, cyclic tetranuclear helicates $Ln_4(\mathbf{87})_4$ or a one-dimensional coordination polymer, in which metal ions and bridging ligands alternate along the sequence, may result depending upon the **87**:Ln ratio and reaction conditions implemented. Reaction of **87** with $Nd(ClO_4)_3$ in a 3:2 ratio in CH_3CN followed by diisopropyl ether diffusion yields crystals suitable for X-ray crystal structure determination. The $[Nd_2(\mathbf{87})_3](ClO_4)_6$ complex contained two nine-coordinate Nd^{III} centres each located within a N_6O_3 site and, contrary to previously discussed helicates above, has a cylindrical (non-helical) 'mesocate' architecture in which the three ligands are arranged in a side-by-side manner. In contrast, reaction of **87** with $Nd(ClO_4)_3$ in a 1:1 ratio in CH_3CN followed by diisopropyl ether diffusion yielded the 4:4 cyclic tetranuclear helicate $[Nd_4(\mathbf{87})_4(H_2O)_{11}(CH_3CN)](ClO_4)12{\cdot}2.5H_2O{\cdot}4CH_3CN$. Luminescence measurements on the Nd^{III} complexes revealed that excitation into the ligand π-π* excited state gives rise to characteristic near-infrared luminescence at 1060 nm.

Research published by Wang and co-workers on the development of multiple Ln^{III} helicate clusters exemplified the significance the templating effect of the counter anion employed can impose upon the stereochemistry of the supramolecular architecture manifested.[194] The bis(tridentate) compound **88** was shown to self-assemble and form a novel hexanuclear Ln^{III} circular helicate ($[La_6\mathbf{88}_6(CH_3O)_3(CH_3OH)_3]^{3+}$) in the presence of $La(ClO_4)_3$, as shown in Figure 12. However, upon addition of $La(NO_3)_3$, which possesses a trigonal planar NO_3^- as opposed to a tetrahedral ClO_4^- counter anion, a tetranuclear stranded helicate complex ($[La_4\mathbf{88}_4(NO_3)]^{3+}$) was preferentially formed. Furthermore, the system was shown to undergo dynamic conversion from the circular helicate to the tetranuclear stranded helicate species upon NO_3^- stimulus. These results signify that simple key factors, such as the size, shape and the binding mode of the counter anion, can play a crucial role in determining the stereochemistry of the resulting self-assembly species.

Both the kinetic and thermodynamic selectivity of the self-assembly process between the bis(tridentate) ligand **89** with the rare earth metals La^{III}, Pr^{III}, Sm^{III}, Yb^{III} and Y^{III} has recently been analysed by Hooley and coworkers.[195] ^1H NMR spectroscopy indicated the formation of triple stranded bimetallic helicates $[\mathbf{89}_3.Ln_2]^{6-}$ in solution following the addition of $Ln(OTf)_3$ (Ln = La^{III}, Pr^{III}, Sm^{III}, Yb^{III} and Y^{III}) to the tetraanionic form of **89** in DMSO in the case of Ln = La^{III}, Pr^{III}, Sm^{III} and Y^{III}; however in the case of Yb^{III} only the 2:2 species was observed. Ligand selectivity for different sized metals was conducted by titrating a second metal ($Ln^A(OTf)_3$) into a preformed 2:3 solution of $[\mathbf{89}_3.Ln^B{}_2]^{6-}$ and noting the extent of displacement, as determined by ^1H NMR. A correlation between effective ionic radius (EIR) of the metal with a preference for displacement of larger ions for smaller ions was revealed - almost complete displacement of La^{III} was observed upon titrating 0.67 equiv. of $Y(OTf)_3$ (EIR = 1.02 Å) to $[\mathbf{89}_3La_2]^{6-}$, for example.

.

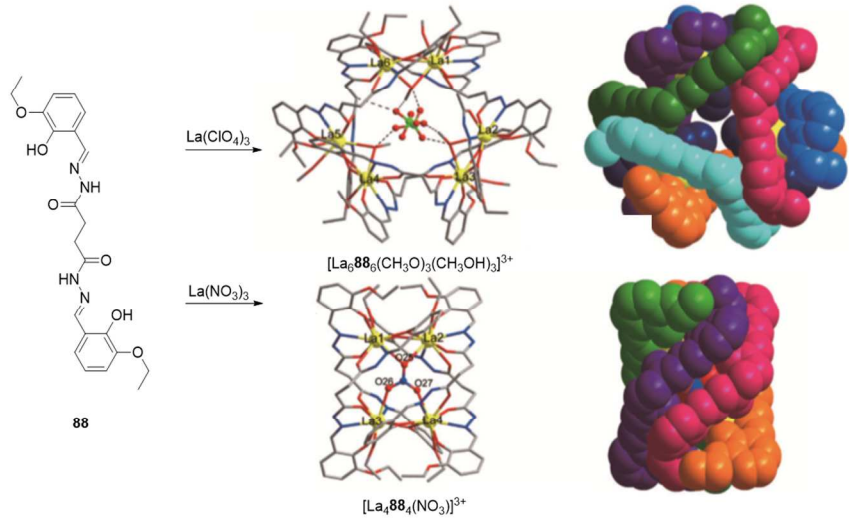

Figure 12. Compound **88** developed for the self-assembly of the circular helicate species $[La_6\mathbf{88}_6(CHO)_3(CH_3OH)_3]^{3+}$ and the tetranuclear stranded helicate complex $[La_4\mathbf{88}_4(NO_3)]^{3+}$. X-ray crystal structures of $[La_6\mathbf{88}_6(CH_3O)(CH_3OH)_3]^{3+}$ and $[La_4\mathbf{88}_4(NO_3)]^{3+}$ are shown. Reproduced from ref. 194 with permission from John Wiley & Sons.

When $La(OTf)_3$ (EIR = 1.18 Å) was added to $[\mathbf{89}_3Y_2]^{6-}$ no displacement was observed. As Δ EIR increased so too did the selectivity for the smaller metal. On the contrary, following thermodynamic equilibration over time the kinetic complex preference was inverted, *i.e.* for the highly selective Y/La system the kinetically disfavoured $[\mathbf{89}_3La_2]^{6-}$ was observed after 3 hrs. Selectivity after equilibration again depended on ΔEIR but the thermodynamic favoured complexes are formed with the larger metal, indicating the added complexity by the presence of a second metal binding site - not only do Coulombic interactions dictate the final complex structure but the added strain, *i.e.* enthalpy of the ligand must also be taken into consideration.

Crystal structures of triple stranded bimetallic helicates, based on the ditopic diamidopyridyl ligand **90** (a secondary product closely related to **62** discussed above), were grown by diffusion of *tert*-butylmethylether into concentrated acetonitrile solutions of $[Ln_2\mathbf{90}_3](ClO_4)_6$ (Ln = Nd^{III}, Eu^{III}, Er^{III}, Eu^{III}) where the three strands are shown to wrap around two Ln ions, possessing a pseudo-D_3 axis passing through the metals.[130] More recently, Hamacek has reported the design and preparation of a homo-octanuclear helicate.[196] ESI mass spectrometry and NMR spectroscopy of the $[Eu_8\mathbf{91}_4]^{24+}$ assembled species confirmed the global tetrahedron structure elucidated by MM in which each hexatopic tripodal ligand **91** is coordinated to six different Eu^{III} centres. Each of the eight Eu^{III} ions are nine coordinated by three diamidopyridyl units on three different ligands in a helical manner. Small angle X-ray scattering (SAXS) measurements were also carried out to gain insight into the solution shape of the octanuclear complex in CH_3CN and correlated well with that calculated from MM while spectrophotometric titrations of **91**

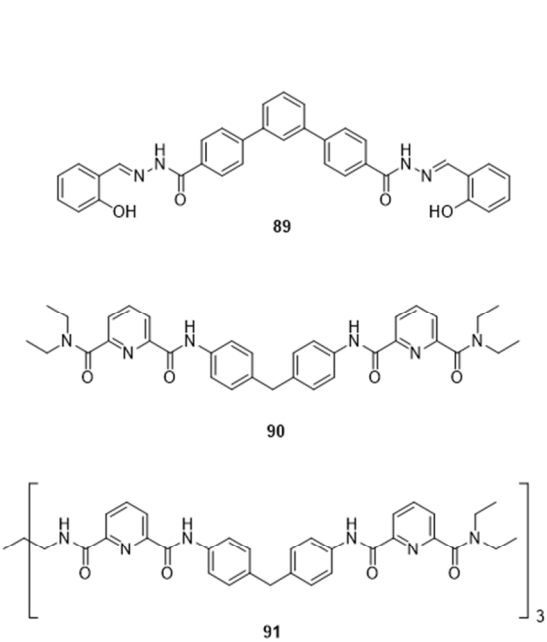

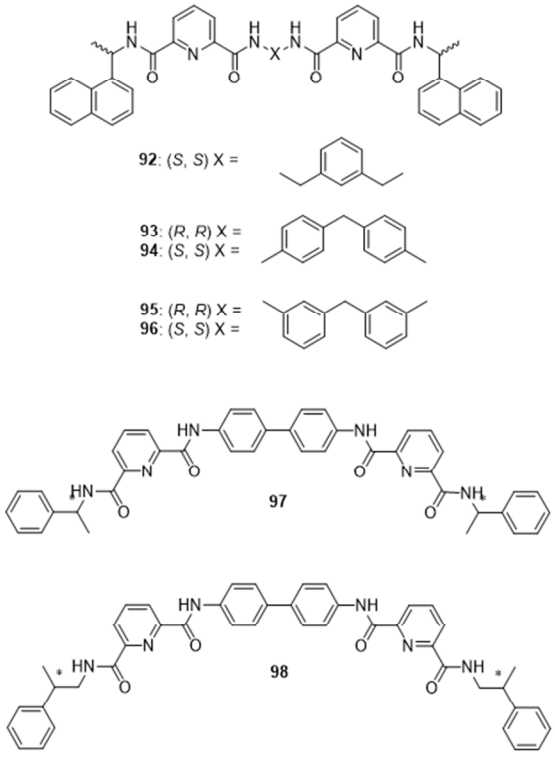

with $Eu(ClO_4)_3$ elucidated the formation of the various stoichiometric species in solution, namely the $Eu\mathbf{91}_2$, $Eu_4\mathbf{91}_4$, $Eu_6\mathbf{91}_4$ and the $Eu_8\mathbf{91}_4$ species, with $[Eu_8\mathbf{91}_4]^{24+}$ possessing a stability constant of $\log_\beta = 62.1$.

Based on a similar framework to that described for **36** and **37**, pre-organised ligands for the Ln^{III}-directed self-assembly of triple stranded homobimetallic helicates ($\mathbf{L}_3$:Ln_2) (**L** = **92** – **93**) have been developed and extensively studied by Gunnlaugsson and coworkers.[197-199] Ligand design of **92** – **96** entailed the incorporation of two 2,6-pyridinedicarboxamide functionalities for bis(tridentate) binding and two chiral naphthalene moieties for sensitisation of the two Ln^{III}, differing by the linking spacer group only. As shown for the chiral ditopic ligand **92** a 1,3-xylene based spacer linked two tridentate diamide pyridyl (NO_2) chelating units together allowing both Ln^{III} ions (Ln^{III} = Sm^{III}, Eu^{III}, Tb^{III}, Lu^{III}) to attain a nine-coordinate binding sphere upon self-assembly, ensuring complete saturation. Evolution of the self-assembled species was monitored spectroscopically as the photophysical properties of the antennae and Ln^{III} were perturbed upon helicate formation. Excitation into the naphthalene antennae (λ_{ex} = 281 nm) and subsequent characteristic Ln^{III}-centred emission confirmed effective sensitisation and thus successful complexation. Fitting of spectroscopic data using non-linear regression analysis indicated that in the presence of 0.2→0.8 equiv. of Eu^{III} the $\mathbf{92}_3$:Eu_2 species was the most dominant in solution with it being formed in over 80% at 0.67 equiv. of Eu^{III}. High thermodynamic stability constants were elucidated for all of the 3:2 and 2:2 **L**:Ln assemblies ($\log\beta_{32} \approx 27$ and $\log\beta_{22} \approx 20$ for Ln^{III} = Sm^{III}, Eu^{III}, Tb^{III}, Lu^{III}) encouraging further studies involving these systems. The inherent chirality of *para*-diphenyl spacer analogues **93** and **94** was exploited for the Eu^{III}-directed formation of one of the first examples of highly stable enantiomerically pure binuclear triple stranded helicates *via* asymmetric induction.[199-201] Solid complexes $Eu_2(\mathbf{L})_3(CF_3SO_3)_6$ (**L** = **93**, **94**) were synthesised by refluxing in CH_3CN and isolated by diethyl ether diffusion. Both ^{1}H NMR and CD spectroscopic studies signified that the complexes were formed as a pair of enantiomers with a high degree of symmetry. The CPL spectra, displaying bands of opposite sign and equal magnitude, further confirming that the chirality of the ligands had indeed been transferred to the Eu^{III} centre upon complexation, giving rise to chiral Eu^{III}-centred emission. The CPL dissymmetry factors of the measured transitions for $Eu_2(\mathbf{L})_3(CF_3SO_3)_6$ (**L** = **93**, **94**) were almost identical in both magnitude and sign to those calculated for the corresponding original mononuclear bundle structures above, whose absolute configurations have been determined by X-ray crystallography. This implied that each bimetallic triple stranded species was formed as a single helical homochiral species possessing either ΔΔ or ΛΛ stereochemistry, respectively.

Variations on this diphenyl linker moiety, namely **95** and **96**, have also been examined with findings suggesting that the stability of the resulting helicate can be greatly affected by the size of the Ln^{III} binding cavity available upon complexation which, in turn, is dictated by the location of connection to the diphenyl spacer. Structural isomers **95** and **96**, which possess two identical binding sites to those of **93** and **94** are linked *via* a *meta*-diphenyl spacer, were also synthesised for the formation of enantiomerically pure bimetallic triple stranded helicates $Eu_2(\mathbf{L})_3$ (**L** = **95**, **96**). Interestingly, a greater stability than that seen for $Eu_2(\mathbf{L})_3$ (**L** = **93**, **94**) was observed for these which is believed to arise from the fact that the central cavity is more "*squeezed*" enabling tighter binding (confirmed using MM2 molecular modelling) of the Eu^{III} upon self-assembly.

With the intention of investigating the importance of the location of the ligand chirality in controlling the chirality of the resulting helicate architecture the two bis(tridentate) diamidopyridyl chiral ligands **97** and **98** (both (*S*, *S*) and (*R*, *R*) isomers of both) were designed.[202] It was found, from ^{1}H NMR titration measurements that addition of $Eu(OTf)_3$ to **97** gave rise to stereoselective formation of one helicate. On the other hand two diastereoselective helicates were formed upon the addition of $Eu(OTf)_3$ to a solution of to **98**, as evidenced again by changes in ^{1}H NMR titration data. Strong cotton effects were observed in the CD spectra of $[Eu_2(\mathbf{97})_3](CF_3SO_3)_6$ whereas a significant decrease in CD signals were seen for $[Eu_2(\mathbf{98})_3](CF_3SO_3)_6$ (both isomers in each case, respectively) – confirming ^{1}H NMR data in which *P*- or *M*-helical chirality is induced to a much lesser extent by **98** than **97**. Furthermore, an X-ray crystal structure of $[Eu_2(\mathbf{97}^{SS})_3](CF_3SO_3)_6$ was obtained - the first X-ray characterized chiral ligand based lanthanide bimetallic triple helicate. Diastereoselectivity is clearly highly sensitive to the chiral point in the ligand structure *i.e.* the ability to effectively transfer chirality to the final helicate structure can be greatly affected by slight structural variations.

Analogous to compounds **63** – **67** above, which were designed for the purpose of assembling cage-type architectures, bis(tridentate) ligands **99** –**103** have also been developed by Duan and co-workers for the Ce^{III}-directed self-assembly of bimetallic

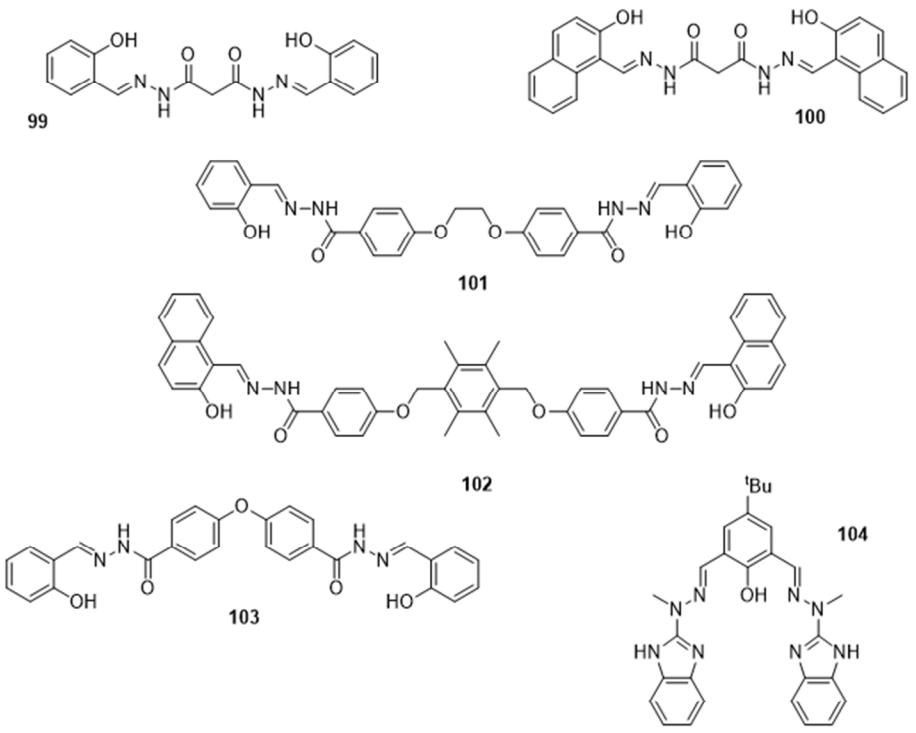

triple stranded helicates, possessing 'lantern-like cavities', for Mg^{2+} chemosensing.[203] The crystal structure of Ce_2**99**$_3$ shows that each Ce^{3+} is residing in a nine coordinate environment in which each metal ion is coordinated to three NO_2 binding units, one on each ligand. The β-diketone linking groups locate inside the structure following helicate formation and where shown to display crown ether recognition behaviour. The ligand-based luminescence band, centred at 465 nm, experienced an 8 fold luminescence enhancement upon the addition of 1 equivalent Mg^{2+} to Ce_2**99**$_3$ in DMF-CH_3CN solution. The titration profile suggested the formation of a 1:1 stoichiometric species in which one Mg^{2+} is encapsulated within the cavity, with an association constant (logK_{ass}) of 5.31. High selectivity of Ce_2**99**$_3$ towards Mg^{2+} over other metals (such as Ca^{2+}, Ba^{2+}, Li^+, Na^+, K^+) was also observed as there were no significant luminescence changes following their addition to a solution of Ce_2**99**$_3$. Mass spectrometry provided evidence of formation of the 1:1 stoichiometric species [Ce_2**100**$_3$. ⊃ $Mg]^{2+}$, as did spectrophotometric measurements were there was a significant ligand-centred luminescence enhancement (centred at λ = 464 nm) upon the addition of Mg^{2+} to a DMF-CH_3CN solution of Ce_2**100**$_3$, with high selectivity for Mg^{2+} - indicating a similar suitable sized cavity for Mg^{2+}. It was concluded from this study that the restricted geometry of the internal cavity in both cases gives rise to its selectivity for Mg^{2+} over other metals.

Bis(tridentate) compounds **101** – **103** were designed for the synthesis of triple stranded bimetallic helicates possessing larger internal cavities than those of Ce_2**99**$_3$ and Ce_2**100**$_3$ above.[204] It was shown that all three ligands again self-assemble *via* Ce^{III}-templation to form helicates possessing cavities with each Ce^{III} coordinated to three NO_2 units. The crystal structure of Ce_2**101**$_3$ confirmed the presence of an internal cavity available for metal ion encapsulation, as before, while a 4.5 fold enhancement in ligand-centred luminescence (centred at λ = 480 nm) was observed upon the addition of 10 equivalents of Mg^{2+} to Ce_2**101**$_3$. The titration profile suggested a host-guest 1:1 stoichiometry, with an

association constant of logK_{ass} = 3.44 calculated, while again selectivity for Mg^{2+} over other metals (such as Ca^{2+}, Ba^{2+}, Li^+, Na^+, K^+ and Al^{3+}) was evident from spectrophotometric investigations. Furthermore, fluorescence studies of the free ligand **101** showed a smaller luminescence enhancement (*ca.* 2 fold enhancement) and decreased selectivity towards Mg^{2+}, following the addition of the ion to a solution of **101**. This again indicates that the constraints of the internal cavity does provide additional size selectivity for Mg^{2+} sensing. A crystal structure of the Ce_2**102**$_3$ species again confirmed the formation of a helical species, similar to Ce_2**101**$_3$. Luminescence measurements elucidated a higher selectivity and competition of Ce_2**102**$_3$ towards Mg^{2+} than seen for Ce_2**101**$_3$with an association constant of logK_{ass} = 4.27 - which was attributed to the cavity size and also to the presence of a cation-π interaction between the Mg^{2+} and the central benzene ring (confirmed by ^{13}C NMR). In the case of the Ce_2**103**$_3$ system the internal cavity was shown, by X-ray crystallography, to be much smaller than those of the systems above. Ce_2**103**$_3$ displayed, by means of fluorescence studies, preferential encapsulation of Al^{III} and thus size selectivity for the smaller cation.

A family of C_3-symmetrical triple stranded bimetallic helicates based on ligand **104** have been reported by Podgajny and coworkers.[205] In this study all [Ln_2**104**$_3$]$(NO_3)_3$, where Ln = Tb^{III},

Dy^{III}, Ho^{III}, Er^{III}, Tm^{III}, Yb^{III}] systems were assembled and characterized by X-ray crystallography, revealing that all compounds were isostructural. Most interesting from this study is that the Er^{III} analogue $[Er_2\mathbf{104}_3](NO_3)_3$ displays DC field induced SMM behaviour, the first reported helicate exhibiting such magnetic behaviour – serving as a platform for the future construction of lanthanide-based SMM helicate architectures.

Employing two metal centres for the formation of functional bimetallic triple stranded helicates has been particularly fruitful in the past decade, with the above examples proving their potential application in a vast array of areas. However, there has also been an acceleration in the generation of functional metal organic frameworks with one of the first Ln^{III} containing MOFs, published in 1999,[206] initiating interest in this field.

3.3 Metal Organic Frameworks (MOFs)

Greatly indebted to the efforts of esteemed researchers such as Yaghi and coworkers,[207,208] the emergence of metal-organic frameworks (MOFs) represents a quantum leap in the progression

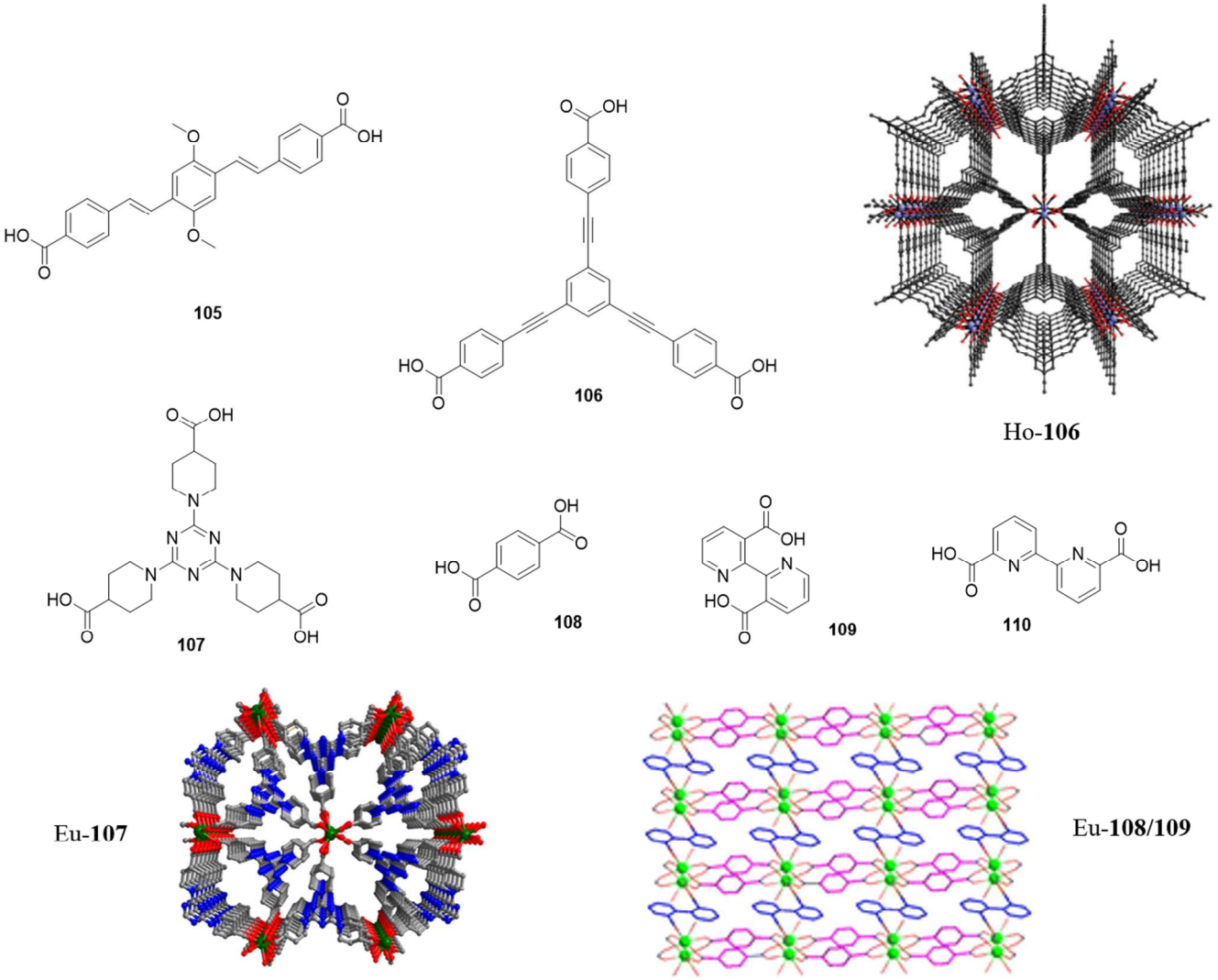

Figure 13. Compounds **105** – **110** developed for the formation of Ln^{III}-containing metal-organic frameworks, extended network crystal structures of Ho-**106** (reproduced from ref. 216 with permission from The Royal Society of Chemistry) and Eu-**107**, with view in the direction of the crystallographic c-axis in both cases, and the 3D framework of Eu-**108**/**109 107** (both Eu-**107** and Eu-**108**/**109 107** reprinted with permission from ref. 53 and 217. Copyright (2013) American Chemical Society).

and evolution of functional multimetallic self-assemblies.[209,210] Constructed by the assembly of metal ions with suitable organic linkers, MOFs comprise a family of crystalline materials famed for ultra-high porosity and huge internal surface areas.[211] The ability to tune pore size and incorporate differing function into the framework makes these structures enormously flexible towards diverse application in molecular storage,[212] drug delivery,[213] catalysis,[214], sensing and so forth. Both the photophysical and magnetic properties inherent to the Ln^{III} ions, coupled with their large varying coordination requirements, has meant that their incorporation into MOFs has become a highly topical area of research in recent times, with the great number of emerging papers reflecting this current interest.

An innovative approach to develop 'barcoded luminescent materials', based on polymetallic Ln-MOFs, has been undertaken by Petoud *et al.*[215] Synthesis of NIR-emitting MOFs was

conducted by reacting the bisbenzoic acid ligand **105** with varying stoichiometries of $Er(NO_3)_3{\cdot}5H_2O$ and $Yb(NO_3)_3{\cdot}5H_2O$ salts yielding four isostructural MOFs: $Er_{0.32}Yb_{0.68}$-**105**, $Er_{0.58}Yb_{0.42}$-**105**, $Er_{0.70}Yb_{0.30}$-**105** and $Er_{0.81}Yb_{0.19}$-**105**. Employing the organic ligand as the sensitizing unit the described Er_xYb_{1-x}−**105** MOFs were shown to simultaneously emit independent NIR signals following excitation at a single wavelength (either 370 nm or 470 nm). By controlling the relative metal stoichiometry the individual emission intensities could be tuned in order to obtain unique NIR barcode fingerprints. A linear correlation was observed between the Er^{III} and Yb^{III} emission band intensities to their respective percentage composition within the MOF. Moreover, MOFs incorporating Er^{III}, Yb^{III} and Nd^{III} were generated, and, as expected, exhibited NIR emission from all three metals, highlighting the potential sophistication of such luminescent 'barcode' materials.

In collaboration with Schmitt and co-workers our research group has developed a series of structurally related visible and NIR-emitting porous Ln-MOFs (Ln = Ho^{III}, Dy^{III}, Er^{III}, Eu^{III}, Tb^{III}, Yb^{III}, Nd^{III}, Sm^{III}).[216] Single crystals of the Ho^{III} analogue ([Ho(**106**)-$(H_2O)_2$]·solv) were grown, displaying an eight coordinate Ho^{III} in which six O donor atoms from separate carboxylate groups from six different deprotonated **106** ligands and two O donor atoms from water molecules were shown to complete the metal coordination sphere. Ho^{III} ions are linked by carboxylate-bridges forming 1D chains which extend parallel to the crystallographic *c*-axis. As shown by the extended network of the crystal structure (see Figure 13), the outer phenyl rings of **106** lie almost perpendicular to the central phenyl ring. This arrangement of ligand binding gives rise to a large (9 Å) and a small channel (5 Å), both with rhombic topology. Furthermore, by replacing the magnetically active Ho^{III} centres with Eu^{III}, Sm^{III} or Nd^{III} ions it was possible to tune the function of the porous network generating luminescent Ln-based MOFs, emitting in the visible and NIR regions. Characteristic Eu^{III}–centred emission was observed for the Eu-**106** MOF, following excitation of the ligand at λ_{ex} = 340 nm, with bands located within the 570-840 nm range for $^5D_0 \rightarrow {}^7F_J$ (J = 0-6). Weak ligand fluorescence was still evident (λ =510 nm) indicating incomplete energy transfer from **106** to Eu^{III}. Emission bands located at 394 and 464 nm, corresponding to the $^5L_6 \leftarrow {}^7F_0$ and $^5D_2 \leftarrow {}^7F_0$ transitions, respectively, and an LMCT at *ca.* 450 nm was also observed. For the Sm-**106** MOF the visible emission bands centred at 561, 595, 642 and 700 nm (associated with the $^4G_{5/2} \rightarrow {}^6H_J$ (J = 5/2, 7/2, 9/2 and 11/2) transitions) were evident, but were weak due to poor sensitization of the metal. The Sm-**106** MOF was also emissive in the NIR region, corresponding to $^4G_{5/2} \rightarrow {}^6F_J$, $^6H_{15/2}$ transitions. Interestingly for the Nd-based MOF it was possible to sensitize the Nd^{III} both indirectly (*via* the antenna effect, λ_{ex} = 360 nm) and directly, resulting in NIR-to-NIR down-conversion photoluminescence.

Implementation of Ln^{III} luminescence as the sensing tool in Ln^{III} based MOFs, as described by the following examples, is experiencing considerable attention at present. Zheng and co-workers have, utilizing ligand **107**, generated a microporous, red-emitting Eu-MOF for the sensing of Fe^{III} and Zn^{II} metal cations. The crystal structure of the Eu−**107** MOF showed the central triazinyl motif of the bridging tricarboxylate ligands directed into the channels of the framework, see Figure 13. The Lewis basic donor nitrogen atoms of **107** were thought to be optimally positioned and readily accessible for interaction with Lewis acidic analytes. Spectroscopic titrations were conducted with a series of metal cations, for which Fe^{III} and Zn^{II} provided the most intriguing results. In contrast, Fe^{III} was found to completely quench the Eu^{III}-centred luminescence, as opposed to Zn^{II} which caused *ca.* 3.5 fold enhancement. In the presence of Fe^{III}, the luminescence lifetime of the **Eu−107** MOF was measured on a nanosecond scale, suggesting that the sensitization of Eu^{III} was essentially blocked upon Fe^{III} coordination. Conversely, a substantial lengthening of the luminescence lifetime was seen upon Zn^{II} addition, which had the supplementary effect of increasing the luminescence quantum yield of the system from 16% to 49%, indicating that electronic perturbation of the structure upon Zn^{II} coordination causes an enhancement in the efficiency of ligand to Eu^{III} energy transfer.[53]

Another series of isostructural luminescent sensing Ln-MOFs (Eu-MOF, Tb-MOF and Eu/Tb-MOFs), which have been designed for the sensing of fluoride anions and small molecule pollutants, are those synthesized *via* a mixed ligand approach under hydrothermal conditions using the two simple ligand precursors **108** and **109**.[217] X-ray crystal structures of [Ln_2(**108**-2H)(**109**-2H)$_2(H_2O)_2]_n$ (Ln = Eu^{III} (Eu-**108**/**109** MOF) and Tb^{III} (Tb -**108**/**109** MOF) reveal a binuclear core where two Ln^{III} ions are four fold linked by two κ^1-κ^1-μ_2 carboxylates from $\mathbf{108}^{2-}$ and two κ^2-κ^1-μ_2 carboxylates from $\mathbf{109}^{2-}$, giving eight coordinate metal ions, which is further connected by $\mathbf{108}^{2-}$ and $\mathbf{109}^{2-}$ to give a 3D network (see Figure 13). Eu-**108**/**109** MOF, Tb-**108**/**109** MOF and the mixed metal MOF systems Eu/Tb-**108**/**109** ($[Eu_{2x}Tb_{2(1-x)}(\mathbf{108}^{2-})(\mathbf{109}^{2-})_2(H_2O)_2]_n$ (x = 0.1 (Eu/Tb-**108**/**109** MOF(a)), 0.3 (Eu/Tb-**108**/**109** MOF(b)), 0.5 (Eu/Tb-**108**/**109** MOF(c)), 0.7 (Eu/Tb-**108**/**109** MOF(d)) and 0.9 (Eu/Tb-**108**/**109** MOF(e))) display high thermal stability, as evidenced by TGA analysis, and, following excitation at 300 nm, Ln^{III}-centred emission. For the mixed metal structures Eu/Tb-**108**/**109** MOF (a-e) luminescence intensity was found to be proportional to its content within the MOF. Suspension-state luminescent experiments were carried out on Eu-**108**/**109** MOF, Tb-**108**/**109** MOF and Eu/Tb-**108**/**109** MOF(a)) in aqueous sodium halide solutions NaCl, NaBr, NaI and NaF revealing a marked quenching effect on the Ln^{III} centred luminescence intensity upon the introduction of F^-. No notable changes were observed for Cl^-, Br^- and I^-, indicating that the MOF is selective for F^- over other halides. Ln^{III} luminescence was also shown to be sensitive to certain small organic molecules such as formaldehyde, acetone and acetonitrile. In the case of Eu-**108**/**109** MOF, formaldehyde caused an increase in emission intensity relative to its concentration, as did acetonitrile in the case of Tb-**108**/**109** MOF and Eu/Tb-**108**/**109** MOF(a). In contrast, a luminescent quenching effect, proportional to the volume ratio of solvent was observed following the addition of acetone to a suspension of Eu-**108**/**109** MOF, Tb-**108**/**109** MOF or Eu/Tb-**108**/**109** MOF(a) in 1,4-dioxane, toluene or formaldehyde, respectively.

Employing the 2,2'-bipyridine-6,6'dicarboxylic acid **110**, an analogue of **109** above, zeolite-like Ln-MOFs (Ln-ZMOF) have been developed for the fluorescent sensing of the ovarian cancer

biomarker lysophosphatidic acid (LPA).[218] In this study pure Eu^{III}–ZMOF ($[Eu_{48}(NO_3)_{48}(\mathbf{110})_{48}]\cdot G_x$ (G = guest)) , Tb^{III}-ZMOF ($^{(}Tb_{48}(NO_3)_{48}(\mathbf{110})_{48}]\cdot G_x$) systems and three mixed-crystal ($Eu^{III}_xTb^{III}_{1-x}$-ZMOF) variants were synthesized. Ln^{III}-centred emission was displayed by all systems, with a gradual decrease in fluorescence intensity upon the addition of increasing concentrations of LPA to a CH_3OH suspension of the Tb-ZMOF (λ = 546 nm monitored). Concurrently, a gradual enhancement was observed upon the addition of increasing concentrations of LPA to a CH_3OH suspension of the Eu-ZMOF (λ = 613 nm monitored); while a similar response in the Eu^{III} and Tb^{III} centred emission was shown for the mixed systems – a linear relationship between integrated intensity and LPA concentration was obtained for $Eu_{0.6}Tb_{0.4}$-ZMOF, confirming it to be a self-calibrating fluorescent indicator. Most notable from this study was that the most sensitive Eu/Tb-ZMOF studied ($Eu_{0.6}Tb_{0.4}$-ZMOF) was able to detect LPA at biologically relevant concentrations (1.4 to 43.3 μM).

Another important contributor to Ln^{III} MOF chemistry is Cahill. Some recent research by this group has involved the development of some of the first examples of a family of reticular Ln-MOFs[219] and also the investigation of lanthanide contraction effects on the structure of a series of Ln-tiophene-2,5-dicarboxylic acid-terpyridine coordination polymers.[220]

As mentioned, many new Ln^{III} luminescent superstructures of this nature have being constructed and as such only a small portion are described above so as to give a flavour of what is currently available and achievable through the use of the *f*-block metals. On the other hand, Ln^{III}-directed templation of interlocked structures, such as rotaxanes, catenanes and knots, remains relatively undeveloped.

3.4 Interlocked structures

Much expertise has been gained by researchers such as Sauvage and Stoddart in the design and assembly of non-covalent interlocked superstructures such as rotaxanes and catenanes in recent times, [221-227] and, more significantly, their role in advancing such systems towards use as molecular switches and in nanoelectronics has been pivotal. Perhaps it is this potential applicability at the nanoscale level, coupled with the attractive features of the lanthanides (optical/magnetic properties) which has inspired the employment of such metals to template the assembly and drive the manifestation of higher order mechanically interlocked structures. To date, only very few novel superstructures which have been accessed in this manner are known.

Faulkner and Beer have utilized the metal templating strategy to assemble the first Ln^{III} containing [2]rotaxanes (where Ln^{III} = Lu^{III} and Eu^{III}).[228] Compound **111** consists of a Ln^{III}-complexed dota cyclen moiety which was integrated into a

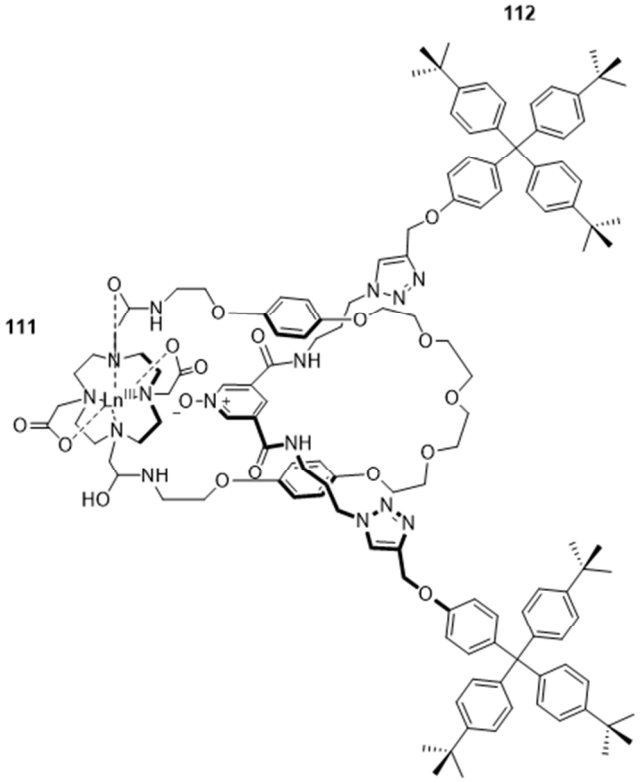

macrocyclic framework. Macrocycle **111** was initially used to form a pseudo-rotaxane by assembling it with an appropriately functionalized pyridine *N*-oxide threading component where the *N*-oxide serves to satisfy the Ln^{III} coordination sphere. The threading unit was then stoppered by a copper(I) catalysed azide-alkyne 'click' reaction yielding **112** and the novel Ln^{III} containing interlocked system Ln.**111**.**112**. The structure was characterized by NMR spectroscopy in which donor-acceptor aromatic stacking interactions between the electron rich hydroquinine groups and the electron deficient pyridine *N*-oxide axle motif are observed.

More recently, the first anion-templated synthesis of a Ln^{III} containing rotaxane was demonstrated where a nitrite anion was used to template initial pseudorotaxane formation by simultaneously coordinating to the lanthanide cation bound within a kinetically stable dota-derived macrocycle **113** and to the hydrogen bonding bis-amide pyridinium motif of the threading precursor.[229] Subsequent stoppering of the interpenetrated assembly allowed for the preparation of the Ln-functionalized [2]rotaxane Ln.**113**.**114** in high yield. Following removal of the anion template the Eu^{III} [2]rotaxane was then shown to recognize and sense fluoride selectively over acetate, nitrite and chloride anions.

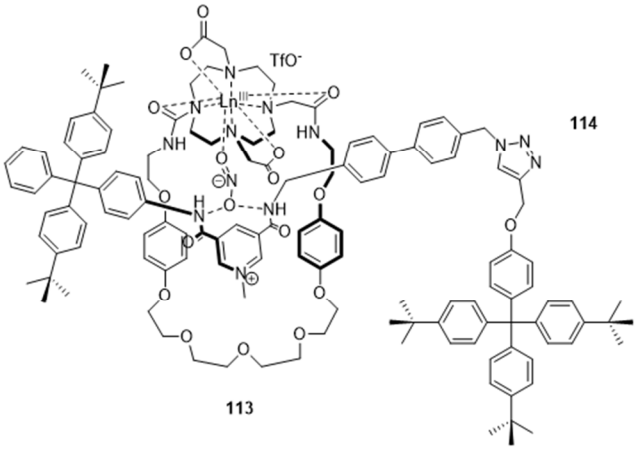

The development of mechanically interlocked structures involving Ln^{III} coordination is also being explored within our laboratory where the first interlocked [2]- and [3]catenanes, which employ the 2,6-diamidopyridyl framework, have been synthesized using Ln^{III}-directed assembly and ring-closing metathesis.[230] As described above, the diaminopyridyl tridentate chelating unit has been studied in great depth forming nine coordinate fully saturated stable 1:3 (Ln:**L**) complexes. A polyethoxy chain bearing a terminal alkene moiety was appended to this core following MM2 force field calculations as it was postulated that catenation was possible for such a system. Complex Eu.**115**$_3$ was synthesized by reacting 0.33 equivalents of $Eu(CF_3SO_3)_3$ with **115** in anhydrous CH_3CN at reflux for 24 hrs. and was evaluated by ^{1}H NMR which showed the presence of a single species in solution. The formation of the Eu.**115**$_3$ assembly was monitored in solution by carrying out spectroscopic titrations and Job's plot analysis in CH_3CN where major changes were observed in both the UV-visible absorption and Eu-centred emission spectra following the addition of 0.33 equiv. of Eu^{III} to **115** *in situ* as the most luminescent 1:3 (Ln:**115**) pre-catenane complex is formed. Non-linear regression analysis of this data elucidated the stoichiometric species formed as well as their corresponding binding constants (log β_{13} = 18.7 ± 0.8 and logβ_{12} = 12.6 ± 0.6 for the 1:3 and 1:2 species, respectively). Ring closing metathesis was then implemented in order to close each macrocycle around the templating metal ion. Mass spectrometry evidenced successful catenation of both the [2]- and [3]catenanes (*m/z* = 1280.42 and 1430.66 for Eu(**115**-2C,2H)$_2$ and 1761.70 and 1919.57 for Eu(**115**-2C,2H)$_3$ (each with one or two $CF_3SO_3^-$, respectively) while ^{1}H NMR confirmed the disappearance of the terminal allyic protons following ring clipping, providing further evidence of the desired system.

A molecular trefoil knot, involving three 2,6-pyridinedicarboxamide ligands **116**, represents another novel example of an impressive interlocked architecture which has been attained *via* Ln^{III} templation.[231] Reaction of the 2,6-diamidopyridyl ligand **116** with 3 equivalents of $Ln(CF_3SO_3)_3$ (Ln= Eu^{III}, Lu^{III}) generated the corresponding $[Ln(\mathbf{116})_3][CF_3SO_3]_3$ complexes in 85% (Eu^{III}) and 90% (Lu^{III}) yields. Mass spectrometry confirmed a 1:3 (Ln:**116**) stoichiometry while ^{1}H NMR indicated that the three ligands were residing in chemically equivalent environments upon coordination to the metal. From the structural analysis of the $[Eu(\mathbf{116})_3)][CF_3SO_3]_3$ complex it is clear that the ligand end groups are in close proximity to the nearest end group of the neighbouring

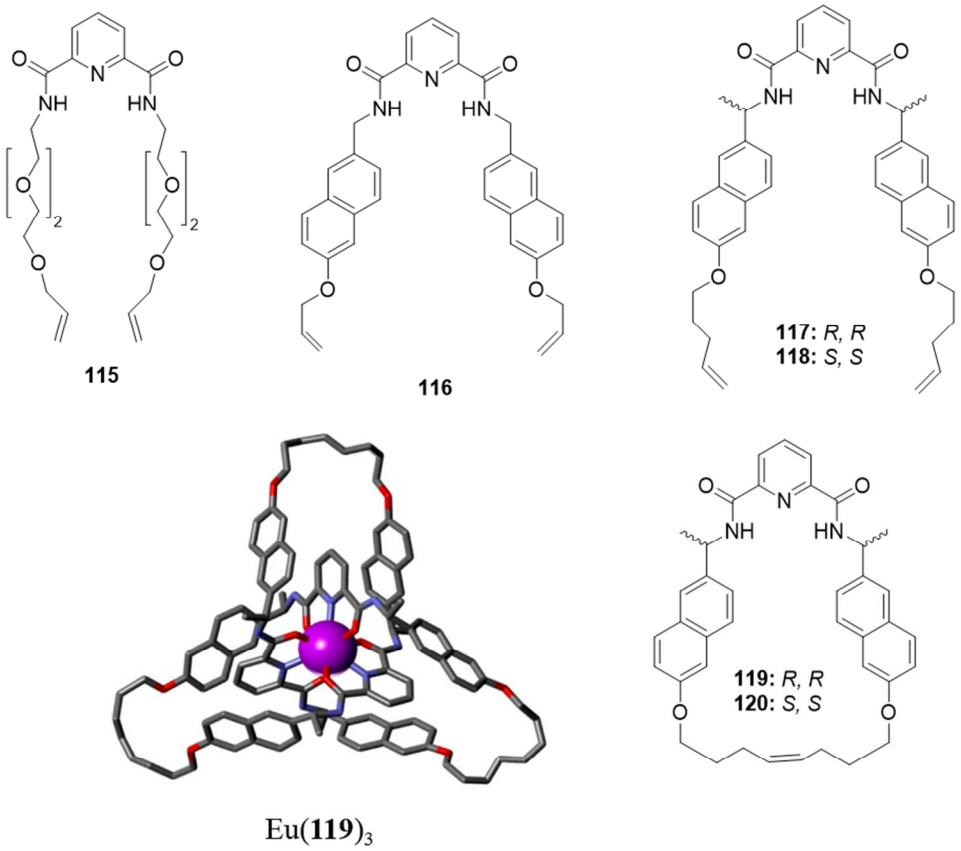

Figure 14. Compounds **115** – **118** for interlocked structure formation and X-ray crystal structure of molecular trefoil knot Eu(**117**-2C,2H)$_3$. Hydrogen atoms, solvent molecules, and counterions are omitted for clarity. The europium atom is shown in purple; nitrogen's, purple; oxygens, red; and carbons, grey.

ligand, enabling the generation a trefoil knot. Upon ring-closing olefin metathesis, this was found to be the case as the major knot species was formed in 58% yield while the topological unknot macrocyclic isomer was afforded in 17% yield. Notably, the trefoil-knot-lanthanide complex displays enhanced stability over the macrocyclic isomer allowing easy separation of the two.

By incorporating two chiral centres, giving symmetric enantiomeric compounds **117** (*R*, *R*) and **118** (*S*, *S*), it was possible to generate trefoil knots of single handedness.[232] In a recent study by Leigh and co-workers, the Ln^{III} metal centre was shown to direct the assembly of compounds **117** and **118** with complete stereoselectivity, where **117** gave rise to a trefoil knot of Λ-handedness and **118** gave rise to a trefoil knot of Δ-handedness only. Self-sorting was not observed when a racemic mixture was used but the influence chirality can impose on the final structure was exemplified, in particular by CD measurements where the induced CD signal of the knot was shown to be 3 times stronger than that of the unknotted macrocycle. Crystals of the Δ-Lu(**120**)$_3$ and Λ-Eu(**119**)$_3$ knots were grown (see Figure 14 for Λ-Eu(**119**)$_3$) showing the molecular topology of the knots where the knotted ligands are wrapped around the metal centre in a helical manner.

4 Conclusions

The aim of this article is to give an updated overview of new and emerging mono- and multimetallic Ln^{III}-directed self-assembled luminescent architectures from ligands based on nitrogen and oxygen containing coordinating moieties While some systems have been extensively studied, others have not, and have only recently been discovered. Many analogues of the dipicolinic acid unit have been developed, for example, for the formation and study of luminescent monometallic complexes in particular. Multimetallic structures, based on the bis(benzimidazole)pyridine helical precursor have also undergone intense scrutiny and derivatization. Chiral integration has been investigated at length by our group and others revealing the important role asymmetry can play in controlling the stereochemistry and thus, luminescent properties of the resulting entity. Interlocked structures, such as rotaxanes, catenanes and trefoil knots, on the other hand, have only recently been explored, opening up a new avenue in the area of molecular switching and nanotechnology in which the advantageous properties of the Ln^{III} metal may be exploited for such purposes.

Bearing in mind that comprehensive overviews by some of the leading researchers within this field have been discussed herein it is evident that a substantial effort is currently ongoing to develop more effective ligand scaffolds in order to widen the scope of these Ln^{III} luminescent systems. These research groups have gained a greater insight into the self-assembly process of a number of different ligand classes' and, in many cases, have fine-tuned the chemical and physical properties of the resultant

superstructure accordingly in order to exploit the versatility these simple building blocks have to offer for their eventual promotion into various disciplines for functional application. Soft matter and solid state fabrication, biological imaging, analyte sensing and SMM behaviour are just some of the examples of potential uses for these assemblies, as have been detailed above. This concise representation describes the broad range of ligands currently available for Ln^{III} -directed self-assembly and highlights the promise of future endeavours within this area of supramolecular chemistry.

5 Acknowledgements

The authors would like to acknowledge the Irish Research Council (IRC) Embark Initiative, IRCSET for postgraduate studentships (DC), We thank Science Foundation Ireland for Financial support (SFI PI Awards 10/IN.1/B2999 and 13/IA/1865, to TG), and TCD School of Chemistry for financial support.

6 Notes and references

[a]*School of Chemistry and Trinity Biomedical Sciences Institute, Trinity College Dublin, University of Dublin, Pearse St, Dublin 2, Ireland; E-mail: barryd5@tcd.ie, gunnlaut@tcd.ie; Fax: +353 1 716 2628; Tel: +353 1 896 3459;*

Reference List

1 K. Binnemans and C. Görller-Walrand, *Chem. Rev.*, 2002, **102**, 2303-2345.
2 K. Binnemans, *Chem. Rev.*, 2009, **109**, 4283-4374.
3 J.-C. G. Bünzli and C. Piguet, *Chem. Rev.*, 2002, **102**, 1897-1928.
4 J.-C. G. Bünzli, *Acc. Chem. Res.*, 2006, **39**, 53-61.
5 J. C. Bünzli, *Chem. Rev.*, 2010, **110**, 2729-2755.
6 A. de Bettencourt-Dias, *Dalton Trans.*, 2007, 2229-2241.
7 S. V. Eliseeva and J. C. Bunzli, *Chem. Soc. Rev.*, 2010, **39**, 189-227.
8 S. V. Eliseeva and J. C. Bunzli, *New J. Chem.*, 2011, **35**, 1165-1176.
9 A. K. Hagan and T. Zuchner, *Anal. Bioanal. Chem.*, 2011, **400**, 2847-2864.
10 S. Pandya, J. H. Yu, and D. Parker, *Dalton Trans.*, 2006, 2757-2766.
11 D. Parker, R. S. Dickins, H. Puschmann, C. Crossland, and J. A. K. Howard, *Chem. Rev.*, 2002, **102**, 1977-2010.
12 S. Shinoda and H. Tsukube, *Analyst (Cambridge, U. K.)*, 2011, **136**, 431-435.
13 A. Thibon and V. r. Pierre, *Anal Bioanal Chem*, 2009, **394**, 107-120.
14 M. D. Ward, *Coord. Chem. Rev.*, 2010, **254**, 2634-2642.
15 W. J. Evans, *Coord. Chem. Rev.*, 2000, **206-207**, 263-283.
16 S. Cotton, Introduction to the Lanthanides, in *Lanthanide and Actinide Chemistry*, John Wiley & Sons, Ltd, 2006, pp. 1-7.
17 J.-C. G. Bünzli, Rare Earth Luminescent Centers in Organic and Biochemical Compounds, in *Spectroscopic Properties of Rare Earths in Optical Materials*, ed. G. K. Liu and B. Jacquier, Springer Verlag, Berlin, 2005, pp. 462-499.
18 J.-C. G. Bünzli and S. V. Eliseeva, Basics of Lanthanide Photophysics, in *Lanthanide Luminescence: Photophysical, Analytical and Biological Aspects*, Springer Berlin Heidelberg, Berlin, 2010, pp. 1-45.
19 J.-C. G. Bünzli and C. Piguet, *Chem. Soc. Rev.*, 2005, **34**, 1048-1077.
20 C. Huang and Z. Bian, Introduction, in *Rare Earth Coordination Chemistry*, John Wiley & Sons, Ltd, 2010, pp. 1-39.
21 T. Gunnlaugsson and J. P. Leonard, *Chem. Commun.*, 2005, 3114-3131.
22 J.-C. Bünzli, *Chem. Lett.*, 2009, **38**, 104-109.
23 C. M. G. dos Santos, A. J. Harte, S. J. Quinn, and T. Gunnlaugsson, *Coord. Chem. Rev.*, 2008, **252**, 2512-2527.
24 S. Faulkner, L. S. Natrajan, W. S. Perry, and D. Sykes, *Dalton Trans.*, 2009, 3890-3899.
25 J.-C. G. Bünzli, Rare Earth Luminescent Centers in Organic and Biochemical Compounds, in *Spectroscopic Properties of Rare Earths in Optical Materials*, ed. R. Hull, J. +. Parisi, R. M. Osgood, Jr., H. Warlimont, G. Liu, and B. Jacquier, Springer Berlin Heidelberg, 2005, pp. 462-499.
26 A. Thibon and V. C. Pierre, *Anal. Bioanal. Chem.*, 2009, **394**, 107-120.
27 S. Comby, D. Imbert, A.-S. Chauvin, and J.-C. G. Bünzli, *Inorg. Chem.*, 2006, **45**, 732-743.
28 L. J. Charbonniere and R. Ziessel, *Helv. Chim. Acta*, 2003, **86**, 3402.
29 G. Tallec, D. Imbert, P. H. Fries, and M. Mazzanti, *Dalton Trans.*, 2010, **39**, 9490-9492.
30 S. Faulkner and B. P. Burton-Pye, *Chem. Commun.*, 2005, 259-261.
31 I. Lukeš, J. Kotek, P. Vojtíšek, and P. Hermann, *Coord. Chem. Rev.*, 2001, **216-217**, 287-312.
32 S. E. Plush, N. A. Clear, J. P. Leonard, A. M. Fanning, and T. Gunnlaugsson, *Dalton Trans.*, 2010, **39**, 3644-3652.
33 C. Lincheneau, E. Quinlan, J. A. Kitchen, T. McCabe, S. E. Matthews, and T. Gunnlaugsson, *Supramol. Chem.*, 2013, **25**, 869-880.
34 J.-M. Lehn, *Science*, 2002, **295**, 2400-2403.
35 D. B. Amabilino and J. F. Stoddart, *Chem. Rev.*, 1995, **95**, 2725-2828.
36 K. S. Chichak, S. J. Cantrill, A. R. Pease, S.-H. Chiu, G. W. V. Cave, J. L. Atwood, and J. F. Stoddart, *Science*, 2004, **304**, 1308-1312.
37 C. O. Dietrich-Buchecker and J. P. Sauvage, *Chem. Rev.*, 1987, **87**, 795-810.
38 N. H. Evans, C. J. Serpell, and P. D. Beer, *Angew. Chem. Int. Ed.*, 2011, **50**, 2507-2510.
39 N. L. Kilah, M. D. Wise, C. J. Serpell, A. L. Thompson, N. G. White, K. E. Christensen, and P. D. Beer, *J. Am. Chem. Soc.*, 2010, **132**, 11893-11895.
40 M. S. Vickers and P. D. Beer, *Chem. Soc. Rev.*, 2007, **36**, 211-225.
41 W.-Y. Sun, M. Yoshizawa, T. Kusukawa, and M. Fujita, *Curr. Opin. Chem. Biol.*, 2002, **6**, 757-764.
42 S. M. Goldup, D. A. Leigh, P. J. Lusby, R. T. McBurney, and A. M. Z. Slawin, *Angew. Chem. Int. Ed.*, 2008, **47**, 6999-7003.
43 A. I. Prikhod'ko, F. Durola, and J. P. Sauvage, *J. Am. Chem. Soc.*, 2007, **130**, 448-449.
44 J. D. Crowley, K. D. Hänni, A.-L. Lee, and D. A. Leigh, *J. Am. Chem. Soc.*, 2007, **129**, 12092-12093.
45 V. Aucagne, J. Berná, J. D. Crowley, S. M. Goldup, K. D. Hänni, D. A. Leigh, P. J. Lusby, V. E. Ronaldson, A. M. Z. Slawin, A. Viterisi, and D. B. Walker, *J. Am. Chem. Soc.*, 2007, **129**, 11950-11963.
46 J. C. Chambron, J.-P. Collin, V. Heitz, D. Jouvenot, J.-M. Kern, P. Mobian, D. Pomeranc, and J.-P. Sauvage, *Eur. J. Org. Chem.*, 2004, 1627-1638.
47 M. Albrecht, O. Osetska, J.-C. G. Bünzli, F. Gumy, and R. Fröhlich, *Chem. Eur. J.*, 2009, **15**, 8791-8799.
48 M. Albrecht, *Z. Anorg. Allg. Chem.*, 2010, **636**, 2198-2204.
49 G. Bozoklu, C. Marchal, C. Gateau, J. Pcaut, D. Imbert, and M. Mazzanti, *Chem. Eur. J.*, 2010, **16**, 6159-6163.
50 D. T. de Lill, A. de Bettencourt-Dias, and C. L. Cahill, *Inorg. Chem.*, 2007, **46**, 3960-3965.
51 V. Fernandez-Moreira, B. Song, V. Sivagnanam, A. S. Chauvin, C. D. B. Vandevyver, M. Gijs, I. Hemmila, H. A. Lehr, and J. C. Bünzli, *Analyst*, 2010, **135**, 42-52.

52 J. P. Leonard, P. Jensen, T. McCabe, J. E. O'Brien, R. D. Peacock, P. E. Kruger, and T. Gunnlaugsson, *J. Am. Chem. Soc.*, 2007, **129**, 10986-10987.
53 Q. Tang, S. Liu, Y. Liu, J. Miao, S. Li, L. Zhang, and Z. Shi, *Inorg. Chem.*, 2013, **52**, 2799-2801.
54 X.-L. Tang, W.-H. Wang, W. Dou, J. Jiang, W.-S. Liu, W.-W. Qin, G.-L. Zhang, H.-R. Zhang, K.-B. Yu, and L.-M. Zheng, *Angew. Chem. Int. Ed.*, 2009, **48**, 3499-3502.
55 E. Terazzi, L. Guénée, J. Varin, B. Bocquet, J.-F. Lemonnier, D. Emery, J. Mareda, and C. Piguet, *Chem. Eur. J.*, 2011, **17**, 184-195.
56 I. Grenthe, *J. Am. Chem. Soc.*, 1961, **83**, 360-364.
57 P. A. Brayshaw, J.-C. G. Bünzli, P. Froidevaux, J. M. Harrowfield, Y. Kim, and A. N. Sobolev, *Inorg. Chem.*, 1995, **34**, 2068-2076.
58 A. Mondry and P. Starynowicz, *J. Alloys Compd.*, 1995, **225**, 367-371.
59 A.-S. Chauvin, F. Gumy, D. Imbert, and J.-C. G. Bünzli, *Spectrosc. Lett.*, 2004, **37**, 517-532; erratum, **2006**, *40(1)*, 193.
60 M. R. George, C. A. Golden, M. C. Grossel, and R. J. Curry, *Inorg. Chem.*, 2006, **45**, 1739-1744.
61 J. B. Lamture, Z. H. Zhou, A. S. Kumar, and T. G. Wensel, *Inorg. Chem.*, 1995, **34**, 864-869.
62 A. L. Gassner, C. Duhot, J. C. G. Bunzli, and A.-S. Chauvin, *Inorg. Chem.*, 2008, **47**, 7802-7812.
63 A. Escande, L. Guene, K.-L. Buchwalder, and C. Piguet, *Inorg. Chem.*, 2009, 1132-1147.
64 G. Muller, J.-C. G. Bünzli, K. J. Schenk, C. Piguet, and G. Hopfgartner, *Inorg. Chem.*, 2001, **40**, 2642-2651.
65 S. Petoud, J.-C. G. Bünzli, K. J. Schenk, and C. Piguet, *Inorg. Chem.*, 1997, **36**, 1345-1353.
66 C. Piguet, A. F. Williams, G. Bernardinelli, E. Moret, and J.-C. G. Bünzli, *Helv. Chim. Acta*, 1992, **75**, 1697-1717.
67 C. Piguet, A. F. Williams, G. Bernardinelli, and J.-C. G. Bünzli, *Inorg. Chem.*, 1993, **32**, 4139-4149.
68 C. Piguet, J. C. G. Bunzli, G. Bernardinelli, C. G. Bochet, and P. Froidevaux, *J. Chem. Soc. , Dalton Trans.*, 1995, 83-97.
69 N. M. Shavaleev, R. Scopelliti, F. Gumy, and J.-C. G. Bünzli, *Inorg. Chem.*, 2009, **48**, 6178-6191.
70 N. M. Shavaleev, F. Gumy, R. Scopelliti, and J.-C. G. Bünzli, *Inorg. Chem.*, 2009, **48**, 5611-5613.
71 N. M. Shavaleev, S. V. Eliseeva, R. Scopelliti, and G. Bunzli J.-C., *Chem. --Eur. J.*, 2009, **15**, 10790-10802.
72 N. M. Shavaleev, S. V. Eliseeva, R. Scopelliti, and J. C. Bu¦ênzli, *Inorg. Chem.*, 2010, **49**, 3927-3936.
73 J. Andres and A. S. Chauvin, *Inorg. Chem.*, 2011, **50**, 10082-10090.
74 A. de Bettencourt-Dias, S. Viswanathan, and A. Rollett, *J. Am. Chem. Soc.*, 2007, **129**, 15436-15437.
75 A. de Bettencourt-Dias, P. S. Barber, S. Viswanathan, D. T. de Lill, A. Rollett, G. Ling, and S. Altun, *Inorg. Chem.*, 2010, **49**, 8848-8861.
76 S. Comby, D. Imbert, A.-S. Chauvin, J.-C. G. Bünzli, L. J. Charbonnière, and R. F. Ziessel, *Inorg. Chem.*, 2004, **43**, 7369-7379.
77 A. Dossing, *Eur. J. Inorg. Chem.*, 2005, 1425-1434.
78 V. M. Mukkala, M. Kwiatkowski, J. Kankare, and H. Takalo, *Helv. Chim. Acta*, 1993, **76**, 893-899.
79 A. Indapurkar, B. Henriksen, J. Tolman, and J. Fletcher, *J. Pharm. Sci.*, 2013, **102**, 2589-2598.
80 E. P. McCarney, J. P. Byrne, B. Twamley, M. Martínez-Calvo, G. Ryan, M. E. Möbius, and T. Gunnlaugsson, *Chem. Commun.*, 2015, **51**, 14123-14126.
81 J. P. Byrne, M. Martínez-Calvo, R. D. Peacock, and T. Gunnlaugsson, *Chem. Eur. J.*, 2015.
82 J. P. Byrne, J. A. Kitchen, and T. Gunnlaugsson, *Chem. Soc. Rev.*, 2014, **43**, 5302-5325.
83 J. P. Byrne, J. A. Kitchen, J. E. O'Brien, R. D. Peacock, and T. Gunnlaugsson, *Inorg. Chem.*, 2015, **54**, 1426-1439.
84 M. A. Halcrow, *New J. Chem.*, 2014, **38**, 1868-1882.
85 M. A. Halcrow, *Coord. Chem. Rev.*, 2005, **249**, 2880-2908.
86 A. P. de Silva, H. Q. N. Gunaratne, and T. E. Rice, *Angew. Chem. Int. Ed. Engl.*, 1996, **35**, 2116-2118.
87 J. K. Molloy, Z. Pillai, J. Sakamoto, P. Ceroni, and G. Bergamini, *Asian J. Org. Chem.*, 2015, **4**, 251-255.
88 J. M. Hamilton, M. J. Anhom, K. A. Oscarson, J. H. Reibenspies, and R. D. Hancock, *Inorg. Chem.*, 2011, **50**, 2764-2770.
89 K. P. Carter, S. J. A. Pope, and C. L. Cahill, *CrystEngComm*, 2014, **16**, 1873-1884.
90 E. S. Andreiadis, R. Demadrill, D. Imbert, J. Pecaut, and M. Mazzanti, *Chem. Eur. J.*, 2009, **15**, 9458-9476.
91 E. S. Andreiadis, D. Imbert, J. Pecaut, R. Demadrill, and M. Mazzanti, *Dalton Trans.*, 2012, **41**, 1268.
92 M. Giraud, E. S. Andreiadis, A. S. Fisyuk, R. Demadrille, J. Pecaut, D. Imbert, and M. Mazzanti, *Inorg. Chem.*, 2008, **47**, 3952-3954.
93 S. Di Pietro, D. Imbert, and M. Mazzanti, *Chem. Commun.*, 2014, **50**, 10323-10326.
94 S. Di Pietro, N. Gautier, D. Imbert, J. Pécaut, and M. Mazzanti, *Dalton Trans.*, 2016, DOI: 10.1039/C5DT04811G.
95 A. Moussa, C. Pham, S. Bommireddy, and G. Muller, *Chirality*, 2009, **21**, 497-506.
96 H. G. Brittain, *Inorg. Chem.*, 1981, **20**, 3007-3013.
97 S. D. Bonsall, M. Houcheime, D. A. Straus, and G. Muller, *Chem. Commun.*, 2007, **3676**.
98 K. T. Hua, J. Xu, E. E. Quiroz, S. Lopez, A. J. Ingram, V. A. Johnson, A. R. Tisch, A. de Bettencourt-Dias, D. A. Straus, and G. Muller, *Inorg. Chem.*, 2012, **51**, 647-660.
99 G. Muller, B. Schmidt, J. Jiricek, G. Hopfgartner, J. P. Riehl, J.-C. G. Bünzli, and C. Piguet, *J. Chem. Soc. , Dalton Trans.*, 2001, 2655-2662.
100 J. Yuasa, T. Ohno, K. Miyata, H. Tsumatori, Y. Hasegawa, and T. Kawai, *J. Am. Chem. Soc.*, 2011, **133**, 9892-9902.
101 K. Do, F. C. Muller, and G. Muller, *J. Phys. Chem. Lett.*, 2008, **112**, 6789-6793.
102 O. Kotova, S. Blasco, B. Twamley, J. E. O'Brien, R. D. Peacock, J. A. Kitchen, M. Martínez-Calvo, and T. Gunnlaugsson, *Chem. Sci.*, 2015, **6**, 457-471.
103 O. Kotova, J. A. Kitchen, C. Lincheneau, R. D. Peacock, and T. Gunnlaugsson, *Chem. Eur. J.*, 2013, **19**, 16181-16186.
104 C. Lincheneau, C. Destribats, D. E. Barry, J. A. Kitchen, R. D. Peacock, and T. Gunnlaugsson, *Dalton Trans.*, 2011, **40**, 12056-12059.
105 M. Han, H.-Y. Zhang, L.-X. Yang, Q. Jiang, and Y. Liu, *Org. Lett.*, 2008, **10**, 5557-5560.
106 C. Lincheneau, R. M. Duke, and T. Gunnlaugsson, *Org. Biomol. Chem.*, 2012, **10**, 6069-6073.
107 D. E. Barry, J. A. Kitchen, M. Albrecht, S. Faulkner, and T. Gunnlaugsson, *Langmuir*, 2013, **29**, 11506-11515.
108 J. A. Kitchen, D. E. Barry, L. Mercs, M. Albrecht, R. D. Peacock, and T. Gunnlaugsson, *Angew. Chem. Int. Ed.*, 2012, **51**, 704-708.
109 C. S. Bonnet, J. Massue, S. J. Quinn, and T. Gunnlaugsson, *Org. Biomol. Chem.*, 2009, **7**, 3074-3078.
110 S. Comby and T. Gunnlaugsson, *ACS Nano*, 2011, **5**, 7184-7197.
111 T. Gunnlaugsson, C. P. McCoy, and F. Stomeo, *Tetrahedron Lett.*, 2004, **45**, 8403-8407.
112 J. Massue, S. J. Quinn, and T. Gunnlaugsson, *J. Am. Chem. Soc.*, 2008, **130**, 6900-6901.
113 N. S. Murray, S. P. Jarvis, and T. Gunnlaugsson, *Chem. Commun.*, 2009, 4959-4961.
114 F. Stomeo, S. E. Plush, and T. Gunnlaugsson, *Chem. Mater.*, 2006, **18**, 4336-4343.
115 L. K. Truman, S. Comby, and T. Gunnlaugsson, *Angew. Chem. Int. Ed.*, 2012, **51**, 9624-9627.
116 M. Martínez-Calvo, O. Kotova, M. E. Möbius, A. P. Bell, T. McCabe, J. J. Boland, and T. Gunnlaugsson, *J. Am. Chem. Soc.*, 2015, **137**, 1983-1992.
117 S. J. Bradberry, A. J. Savyasachi, R. D. Peacock, and T. Gunnlaugsson, *Faraday Discuss.*, 2015, **185**, 413-431.

118 S. J. Bradberry, J. P. Byrne, C. P. McCoy, and T. Gunnlaugsson, *Chem. Commun.*, 2015, **51**, 16565-16568.
119 O. Kotova, R. Daly, C. M. G. dos Santos, M. Boese, P. E. Kruger, J. J. Boland, and T. Gunnlaugsson, *Angew. Chem. Int. Ed.*, 2012, **51**, 7208-7212.
120 R. Daly, O. Kotova, M. Boese, T. Gunnlaugsson, and J. J. Boland, *ACS Nano*, 2013, **7**, 4838-4845.
121 O. Kotova, R. Daly, C. M. G. dos Santos, P. E. Kruger, J. J. Boland, and T. Gunnlaugsson, *Inorg. Chem.*, 2015, **54**, 7735-7741.
122 S. H. Jung, K.-Y. Kwon, and J. H. Jung, *Chem. Commun.*, 2015, **51**, 952-955.
123 H. S. Jung, J. Jeon, H. Kim, J. Jaworski, and J. H. Jung, *J. Am. Chem. Soc.*, 2014, **136**, 6446-6452.
124 G. Bozoklu, C. Gateau, D. Imbert, J. Pécaut, K. Robeyns, Y. Filinchuk, F. Memon, G. Muller, and M. Mazzanti, *J. Am. Chem. Soc.*, 2012, **134**, 8372-8375.
125 J. Hamacek, G. Bernardinelli, and Y. Filinchuk, *Eur. J. Inorg. Chem.*, 2008, 3419-3422.
126 J. Hamacek, C. Besnard, T. Penhouet, and P. Y. Morgantini, *Chem. --Eur. J.*, 2011, **17**, 6753-6764.
127 B. E. Aroussi, L. Guénée, P. Pal, and J. Hamacek, *Inorg. Chem.*, 2011, **50**, 8588-8597.
128 J. Hamacek, D. Poggiali, S. Zebret, B. E. Aroussi, M. W. Schneider, and M. Mastalerz, *Chem. Commun.*, 2012, **48**, 1281-1283.
129 S. Zebret, C. Besnard, G. Bernardinelli, and J. Hamacek, *Eur. J. Inorg. Chem.*, 2012, 2409-2417.
130 B. E. Aroussi, S. Zebret, C. Besnard, P. Perrotter, and J. Hamacek, *J. Am. Chem. Soc.*, 2011, **133**, 10764-10767.
131 Y. Liu, X. Wu, C. He, Y. Jiao, and C. Duan, *Chem. Commun.*, 2009, 7554-7556.
132 Y. Jiao, J. Wang, P. Wu, L. Zhao, C. He, J. Zhang, and C. Duan, *Chem. --Eur. J.*, 2014, **20**, 2224-2231.
133 L.-L. Yan, C.-H. Tan, G.-L. Zhang, L.-P. Zhou, J.-C. Bünzli, and Q.-F. Sun, *J. Am. Chem. Soc.*, 2015, **137**, 8550-8555.
134 L. N. Dawe, T. S. M. Abedin, and L. K. Thompson, *Dalton Trans.*, 2008, 1661-1675.
135 V. A. Milway, S. M. T. Abedin, V. Neil, T. L. Kelly, L. N. Dawe, S. K. Dey, D. W. Thompson, D. O. Miller, M. S. Alam, P. Müller, and L. K. Thompson, *Dalton Trans.*, 2006, 2835-2851.
136 L. N. Dawe, K. V. Shuvaev, and L. K. Thompson, *Inorg. Chem.*, 2009, **48**, 3323-3341.
137 M. U. Anwar, S. S. Tandon, L. N. Dawe, F. Habib, M. Murugesu, and L. K. Thompson, *Inorg. Chem.*, 2012, **51**, 1028-1034.
138 M. U. Anwar, L. K. Thompson, L. N. Dawe, F. Habib, and M. Murugesu, *Chem. Commun.*, 2012, **48**, 4576-4578.
139 N. M. Randell, M. U. Anwar, M. W. Drover, L. N. Dawe, and L. K. Thompson, *Inorg. Chem.*, 2013, **52**, 6731-6742.
140 L. K. Thompson and L. N. Dawe, *Coord. Chem. Rev.*, 2015, **289-290**, 13-31.
141 J. Wu, L. Zhao, M. Guo, and J. Tang, *Chem. Commun.*, 2015.
142 J. D. Rinehart, M. Fang, W. J. Evans, and J. R. Long, *Nat Chem*, 2011, **3**, 538-542.
143 J. Tang, I. Hewitt, N. T. Madhu, G. Chastanet, W. Wernsdorrfer, C. E. Anson, C. Benelli, R. Sessoli, and A. K. Powell, *Angew. Chem. Int. Ed.*, 2006, **45**, 1729-1733.
144 I. J. Hewitt, J. Tang, N. T. Madhu, C. E. Anson, Y. Lan, J. Luzon, M. Etienne, R. Sessoli, and A. K. Powell, *Angew. Chem. Int. Ed.*, 2010, **49**, 6352-6356.
145 Y.-N. Guo, G.-F. Xu, W. Wernsdorrfer, L. Ungur, Y. Guo, J. Tang, H.-J. Zhang, L. F. Chibotaru, and A. K. Powell, *J. Am. Chem. Soc.*, 2011, **133**, 11948-11951.
146 P.-H. Lin, T. J. Burchell, L. Ungur, L. F. Chibotaru, W. Wernsdorrfer, and M. Murugesu, *Angew. Chem. Int. Ed.*, 2009, **48**, 9489-9492.
147 F. Duan, L. Liu, C. Qiao, and H. Yang, *Inorg. Chem. Commun.*, 2015, **55**, 120-122.
148 M. Maity, M. C. Majee, S. Kundu, S. K. Samanta, and K. C. Sañudo, *Inorg. Chem.*, 2015, **54**, 9715-9726.
149 A.-J. Hutchings, F. Habib, R. J. Holmberg, I. Korobkov, and M. Murugesu, *Inorg. Chem.*, 2015, **53**, 2102-2112.
150 E. C. Constable, *Tetrahedron*, 1992, **48**, 10013-10059.
151 E. C. Constable, A. J. Edwards, P. R. Raithby, and J. V. Walker, *Angew. Chem. Int. Ed.*, 1993, **32**, 1465-1467.
152 J.-M. Lehn and A. Rigault, *Angew. Chem. Int. Ed.*, 1988, **27**, 1095-1097.
153 J.-M. Lehn, A. Rigault, J. Siegel, J. Harrowfield, B. Chevrier, and D. Moras, *Proc Natl Acad Sci U S A*, 1987, **84**, 2565-2569.
154 R. Krämer, J.-M. Lehn, and A. Marquis-Rigault, *Proc Natl Acad Sci U S A*, 1993, **90**, 5394-5398.
155 C. O. Dietrich-Buchecker, J. Guilhem, C. Pascard, and J.-P. Sauvage, *Angew. Chem. Int. Ed.*, 1990, **29**, 1154-1156.
156 T. Gunnlaugsson and F. Stomeo, *Org. Biomol. Chem.*, 2007, **5**, 1999-2009.
157 C. Lincheneau, F. Stomeo, S. Comby, and T. Gunnlaugsson, *Aust. J. Chem.*, 2011, **64**, 1315-1326.
158 A. F. Williams, C. Piguet, and G. Bernardinelli, *Angew. Chem. , Int. Ed.*, 1991, **30**, 1490-1492.
159 G. Bernardinelli, C. Piguet, and A. F. Williams, *Angew. Chem. Int. Ed.*, 1992, **31**, 1622-1624.
160 C. Piguet, J.-C. G. Bünzli, G. Bernardinelli, G. Hopfgartner, and A. F. Williams, *J. Am. Chem. Soc.*, 1993, **115**, 8197-8206.
161 J. Hamacek, S. Blanc, M. Elhabiri, E. Leize, A. Van Dorsselaer, C. Piguet, and A.-M. Albrecht-Gary, *J. Am. Chem. Soc.*, 2003, **125**, 1541-1550.
162 C. Piguet, G. Hopfgartner, A. F. Williams, and J.-C. G. Bünzli, *J. Chem. Soc. ,Chem. Commun.*, 1995, 491-493.
163 C. Piguet, G. Bernardinelli, J.-C. G. Bünzli, S. Petoud, and G. Hopfgartner, *J. Chem. Soc. , Chem. Commun.*, 1995, 2575-2577.
164 N. André, R. Scopelliti, G. Hopfgartner, C. Piguet, and J.-C. G. Bünzli, *Chem. Commun.*, 2002, 214-215.
165 N. André, T. B. Jensen, R. Scopelliti, D. Imbert, M. Elhabiri, G. Hopfgartner, C. Piguet, and J.-C. G. Bünzli, *Inorg. Chem.*, 2004, **43**, 515-529.
166 S. Floquet, M. Borkovec, G. Bernardinelli, A. Pinto, L. A. Leuthold, G. Hopfgartner, D. Imbert, and J.-C. G. Bünzli, *Chem. --Eur. J.*, 2004, **10**, 1091-1105.
167 S. Floquet, N. Ouali, B. Bocquet, G. Bernardinelli, D. Imbert, J.-C. G. Bünzli, G. Hopfgartner, and C. Piguet, *Chem. --Eur. J.*, 2003, 1860-1875.
168 N. Dalla-Favera, J. Hamacek, M. Borkovec, D. Jeannerat, F. Gumy, J.-C. Bünzli, G. Ercolani, and C. Piguet, *Chem. Eur. J.*, 2008, **14**, 2994-3005.
169 N. Dalla-Favera, J. Hamacek, M. Borkovec, D. Jeannerat, G. Ercolani, and C. Piguet, *Inorg. Chem.*, 2007, **46**, 9312-9322.
170 M. Cantuel, F. Gumy, J.-C. G. Bünzli, and C. Piguet, *Dalton Trans.*, 2006, 2647-2660.
171 T. Riis-Johannessen, G. Bernardinelli, Y. Filinchuk, S. Clifford, N. D. Favera, and C. Piguet, *Inorg. Chem.*, 2009, **48**, 5512-5525.
172 J.-C. G. Bünzli, A.-S. Chauvin, C. D. B. Vandevyver, B. Song, and S. Comby, *Ann. N. Y. Acad. Sci.*, 2008, **1130**, 97-105.
173 A.-S. Chauvin, S. Comby, B. Song, C. D. B. Vandevyver, and J.-C. G. Bünzli, *Chem. Eur. J.*, 2007, **13**, 9515-9526.
174 E. Deiters, B. Song, A. S. Chauvin, C. D. B. Vandevyver, F. Gumy, and J.-C. G. Bünzli, *Chem. Eur. J.*, 2009, **15**, 885-900.
175 S. V. Eliseeva, G. Auböck, F. van Mourik, A. Cannizzo, B. Song, E. Deiters, A. S. Chauvin, M. Chergui, and J.-C. Bünzli, *J. Phys. Chem. B*, 2010, **114**, 2932-2937.
176 S. V. Eliseeva, B. Song, C. D. B. Vandevyver, A. S. Chauvin, J. B. Wacker, and J.-C. G. Bünzli, *New J. Chem.*, 2010, **34**, 2915-2921.
177 B. Song, C. D. B. Vandevyver, E. Deiters, A. S. Chauvin, I. Hemmila, and J.-C. G. Bünzli, *Analyst*, 2008, **133**.
178 B. Song, V. Sivagnanam, C. D. B. Vandevyver, I. Hemmila, H. A. Lehr, M. A. M. Gijs, and J. C. Bunzli, *Analyst*, 2009, **134**, 1991-1993.
179 C. D. B. Vandevyver, A.-S. Chauvin, S. Comby, and J.-C. G. Bünzli, *Chem. Commun.*, 2007, 1716-1718.

180 N. Martin, J.-C. G. Bünzli, V. McKee, C. Piguet, and G. Hopfgartner, *Inorg. Chem.*, 1998, **37**, 577-589.
181 M. Elhabiri, R. Scopelliti, J.-C. G. Bünzli, and C. Piguet, *Chem. Commun.*, 1998, 2347-2349.
182 M. Elhabiri, R. Scopelliti, J.-C. G. Bünzli, and C. Piguet, *J. Am. Chem. Soc.*, 1999, **121**, 10747-10762.
183 M. Elhabiri, J. Hamacek, J.-C. G. Bünzli, and A.-M. Albrecht-Gary, *Eur. J. Inorg. Chem.*, 2004, 51-62.
184 B. Song, C. D. B. Vandevyver, A. S. Chauvin, and J.-C. G. Bünzli, *Org. Biomol. Chem.*, 2008, **6**, 4125-4133.
185 C. Piguet, M. Borkovec, J. Hamacek, and K. Zeckert, *Coord. Chem. Rev.*, 2005, **249**, 705-729.
186 M. Borkovec, J. Hamacek, and C. Piguet, *Dalton Trans.*, 2004, 4096-4105.
187 C. Piguet, *Chem. Commun.*, 2010, **46**, 6209-6231.
188 J. Hamacek, M. Borkovec, and C. Piguet, *Chem. --Eur. J.*, 2005, **11**, 5217-5226.
189 J. Hamacek, M. Borkovec, and C. Piguet, *Chem. --Eur. J.*, 2005, **11**, 5227-5237.
190 A. P. Bassett, S. W. Magennis, P. B. Glover, D. J. Lewis, N. Spencer, S. Parsons, R. M. Williams, L. De Cola, and Z. Pikramenou, *J. Am. Chem. Soc.*, 2004, **126**, 9413-9424.
191 M. Albrecht, R. Fröhlich, J.-C. G. Bünzli, A. Aebischer, F. Gumy, and J. Hamacek, *J. Am. Chem. Soc.*, 2007, 14178-14179.
192 M. Albrecht and O. Osetska, *Eur. J. Inorg. Chem.*, 2010, **2010**, 4678-4682.
193 T. K. Ronson, H. Adams, L. P. Harding, S. J. A. Pope, D. Sykes, S. Faulkner, and M. D. Ward, *Dalton Trans.*, 2007, 1006-1022.
194 B. Wang, Z. Zang, H. Wang, W. Dou, X. Tang, W. Liu, Y. Shao, J. Ma, Y. Li, and J. Zhou, *Angew. Chem. Int. Ed.*, 2013, **52**, 3756-3759.
195 A. M. Johnson, M. C. Young, X. Zhang, R. R. Julian, and R. J. Hooley, *J. Am. Chem. Soc.*, 2013, **135**, 17723-17726.
196 S. Zebret, E. Vögele, T. Klumpler, and J. Hamacek, *Chem. --Eur. J.*, 2015, **21**, 6695-6699.
197 S. Comby, F. Stomeo, C. P. McCoy, and T. Gunnlaugsson, *Helv. Chim. Acta*, 2009, **92**, 2461-2473.
198 C. Lincheneau, R. D. Peacock, and T. Gunnlaugsson, *Chem. Asian J.*, 2010, **5**, 500-504.
199 F. Stomeo, C. Lincheneau, J. P. Leonard, J. E. O'Brien, R. D. Peacock, C. P. McCoy, and T. Gunnlaugsson, *J. Am. Chem. Soc.*, 2009, **131**, 9636-9637.
200 M. Albrecht, S. Schmid, S. Dehn, C. Wickleder, S. Zhang, A. P. Bassett, Z. Pikramenou, and R. Frohlichd, *New J. Chem.*, 2007, **31**, 1755-1762.
201 M. Cantuel, G. Bernardinelli, G. Muller, J. P. Riehl, and C. Piguet, *Inorg. Chem.*, 2004, **43**, 1840-1849.
202 C.-T. Yeung, W. T. K. Chan, S.-C. Yan, K.-L. Yu, K.-H. Yim, W.-T. Wong, and G.-L. Law, *Chem. Commun.*, 2015, **51**, 592-595.
203 X. Zhu, C. He, D. Dong, Y. Liu, and C. Duan, *Dalton Trans.*, 2010, **39**, 10051-10055.
204 L. Zhao, Y. Liu, C. He, J. Wang, and C. Duan, *Dalton Trans.*, 2014, **43**, 335-343.
205 A. Gorczynski, M. Kubicki, D. Pinkowicz, R. Pelka, V. Patroniak, and R. Podgajny, *Dalton Trans.*, 2015, **44**, 16833-16839.
206 T. M. Reineke, M. Eddaoudi, M. Fehr, D. Kelley, and O. M. Yaghi, *J. Am. Chem. Soc.*, 1999, **121**, 1651-1657.
207 O. M. Yaghi, M. O'Keeffe, N. W. Ockwig, H. K. Chae, M. Eddaoudi, and J. Kim, *Nature*, 2003, **423**, 705.
208 M. Eddaoudi, D. B. Moler, H. Li, B. Chen, T. M. Reineke, and O. M. Yaghi, *Acc. Chem. Res.*, 2001, **34**, 319-330.
209 Metal-Organic Frameworks. Chemical Reviews 112[2]. 2012.
Ref Type: Journal (Full)
210 H. Furukawa, K. E. Cordova, M. O'Keeffe, and O. M. Yaghi, *Science*, 2013, **341**, 6149.
211 T. R. Cook, Y.-R. Zheng, and P. J. Stang, *Chem. Rev.*, 2013, **113**, 734-777.
212 N. L. Rosi, J. Eckert, M. Eddaoudi, D. T. Vodak, J. Kim, M. O'Keeffe, and O. M. Yaghi, *Science*, 2003, **300**, 1127.
213 P. Horcajada, R. Gref, T. Baati, P. K. Allan, G. Maurin, P. Couvreur, G. Ferey, R. E. Morris, and C. Serre, *Chem. Rev.*, 2012, **112**, 1232-1268.
214 Z. Wang, G. Chen, and K. Ding, *Chem. Rev.*, 2009, **109**, 322-359.
215 K. A. White, D. A. Chengelis, K. A. Gogick, J. Stehman, N. L. Rosi, and S. ü. Petoud, *J. Am. Chem. Soc.*, 2009, **131**, 18069-18071.
216 G. Tobin, S. Comby, N. Zhu, R. Clérac, T. Gunnlaugsson, and W. Schmitt, *Chem. Commun.*, 2015, **51**, 13313-13316.
217 J.-M. Zhou, W. Shi, N. Xu, and P. Cheng, *Inorg. Chem.*, 2013, **52**, 8082-8090.
218 S.-Y. Zhang, W. Shi, P. Cheng, and M. J. Zaworotko, *J. Am. Chem. Soc.*, 2015, **137**, 12203-12206.
219 Z. Min, M. A. Singh-Wilmot, C. L. Cahill, M. Andrews, and R. Taylor, *Eur. J. Inorg. Chem.*, 2012, 4419-4426.
220 K. P. Carter, C. H. F. Zulato, E. M. Rodrigues, S. J. A. Pope, F. A. Sigoli, and C. L. Cahill, *Dalton Trans.*, 2015, **44**, 15843-15854.
221 M. Cesario, Dietrich-Buchecker, C.O., J. Guilhem, and C. Sauvage, *J. Chem. Soc. ,Chem. Commun.*, 1985, 244-247.
222 C. O. Dietrich-Buchecker, C. Sauvage, and J. Weiss, *Tetrahedron Lett.*, 1986, **27**, 2257-2260.
223 J. A. Bravo, F. M. Raymo, J. F. Stoddart, A. J. P. White, and D. J. Wiliams, *Eur*, 1998, 2565-2571.
224 J. F. Stoddart and S.-R. Tseng, *Proc. Ntl. Acad. Sci. USA*, 2002, **99**, 4797-4800.
225 T. Iijima, S. A. Vignon, H. R. Tseng, T. Jarrosson, J. K. M. Sanders, F. Marchioni, M. Venturi, E. Apostoli, V. Balzani, and J. F. Stoddart, *Chem. --Eur. J.*, 2004, **10**, 6375-6392.
226 J. P. Sauvage and C. Dietrich-Buchecker, Molecular Catenanes, Rotaxanes and Knots: A Journey Through the World of Molecular Topology, John Wiley & Sons, 2008.
227 F. M. Raymo and J. F. Stoddart, Organic Template-Directed Syntheses of Catenanes, Rotaxanes, and Knots , John Wiley & Sons, 2008, pp. 143-176.
228 F. Zapata, O. A. Blackburn, M. J. Langton, S. Faulkner, and P. D. Beer, *Chem. Commun.*, 2013, **49**, 8157-8159.
229 M. J. Langton, O. A. Blackburn, T. Lang, S. Faulkner, and P. D. Beer, *Angew. Chem. Int. Ed.*, 2014, **53**, 11463-11466.
230 C. Lincheneau, B. Jean-Denis, and T. Gunnlaugsson, *Chem. Commun.*, 2014, **50**, 2857-2860.
231 J.-F. Ayme, G. Gil-Ramírez, D. A. Leigh, J.-F. Lemonnier, A. Markevicius, C. A. Muryn, and G. Zhang, *J. Am. Chem. Soc.*, 2014, **136**, 13142-13145.
232 G. Zhang, G. Gil-Ramírez, A. Markevicius, C. Browne, I. J. Vitorica-Yrezabal, and D. A. Leigh, *J. Am. Chem. Soc.*, 2015, **137**, 10437-10442.